Supporting Information

A Novel Lactam-Based AIE Building Block for High-Performance Deep-Blue Electroluminescent Materials

Luyao Liu, [a, 1] *Jingli Lou,* [a, 1] *Jiaxing Wan,* [a] *Yin Li,* [b] *Hao Xiong,* [a] *Yu Huang,* [a] *Dezhi Yang,* [a] *Han Zhang,* [c,] * *Ben Zhong Tang* [d] *and Zhiming Wang* [a,] *

a L. Liu, J. Lou, J. Wan, H, Xiong, Y. Huang, Prof D. Yang, Prof. Z. Wang
AIE Institute, State Key Laboratory of Luminescent Materials and Devices, Center for Aggregation-Induced Emission, South China University of Technology (SCUT), Guangzhou 510640, China
E-mail: wangzhiming@scut.edu.cn

b Dr. Y. Li
Jianghan University, Institute of Intelligent Sport and Proactive Health, School of Physical Education, Wuhan, 430056, China

c Dr. H. Zhang
Department of Chemistry, Hong Kong Branch of Chinese National Engineering Research Center for Tissue Restoration and Reconstruction, The Hong Kong University of Science and Technology, Clear Water Bay, Kowloon, Hong Kong 999077, China.
E-mail: cheungham@ust.hk

d Prof. B. Z. Tang
Shenzhen Institute of Aggregate Science and Technology, School of Science and Engineering, The Chinese University of Hong Kong, Shenzhen, Shenzhen 518172, China

[1] Luyao Liu and Jingli Lou contributed equally to this work.

Contents

S-1 Materials and Measurment

All the reagents and solvents were purchased from commercial sources and used as received. The final products were subjected to vacuum sublimation to further improve purity before photoluminescence (PL) and electroluminescnce (EL) properties investigations. ^{1}H and ^{13}C NMR spectra were recorded on a Bruker AV 500 spectrometer in CH_2Cl_2 at room temperature. High resolution mass spectra (HRMS) were tested on Agilent1290/Bruker maXis impact. Thermogravimetric analysis (TGA) was performed on a TA TGA Q5000 from 30 ℃ to 800 ℃ under dry nitrogen at a heating rate of 10 °C min^{-1}. The differential scanning calorimetry (DSC) analysis was carried out on a DSC Q1000 from 30 ℃ to 300 ℃ under dry nitrogen at a heating rate of 5 °C min^{-1}. Cyclic voltammetry (CV) were performed on a CHI 610E A14297 in a solution of tetra-n-butylammonium hexafluorophosphate (Bu_4NPF_6) (0.1 M) in dichloromethane (DCM) or dimethylformamide (DMF) at a scan rate of 100 mV s^{-1}, using a platinum wire as the auxiliary electrode, a glass carbon disk as the working electrode and Ag/Ag^+ as the reference electrode. Ionization Potential (IP_{CV}) = [$E_{OX} - E_{1/2}(Fc/Fc^+) + 4.8$] eV, Electron Affinities (EA_{CV}) = [$E_{red} - E_{1/2}(Fc/Fc^+) + 4.8$] eV, where E_{ox} and E_{red} represent the onset oxidation potential and the reduction potential relative to Fc/Fc^+ (4.8 eV), respectively, and $E_{1/2}$ (Fc/Fc^+) represents the calibrated value. UV-vis absorption spectra were recorded with a Shimadzu UV-2600 spectrophotometer. Measurements of PL spectra were carried out on Horiba Fluoromax-4 spectrofluorometer. Fluorescence quantum yields in solutions and solid films were measured using a Hamamatsu absolute PL quantum yield spectrometer C11347 Quantaurus QY. Fluorescence lifetimes were determined on an Edinburgh FLS1000 spectrometer.

S-2 Experimental Section

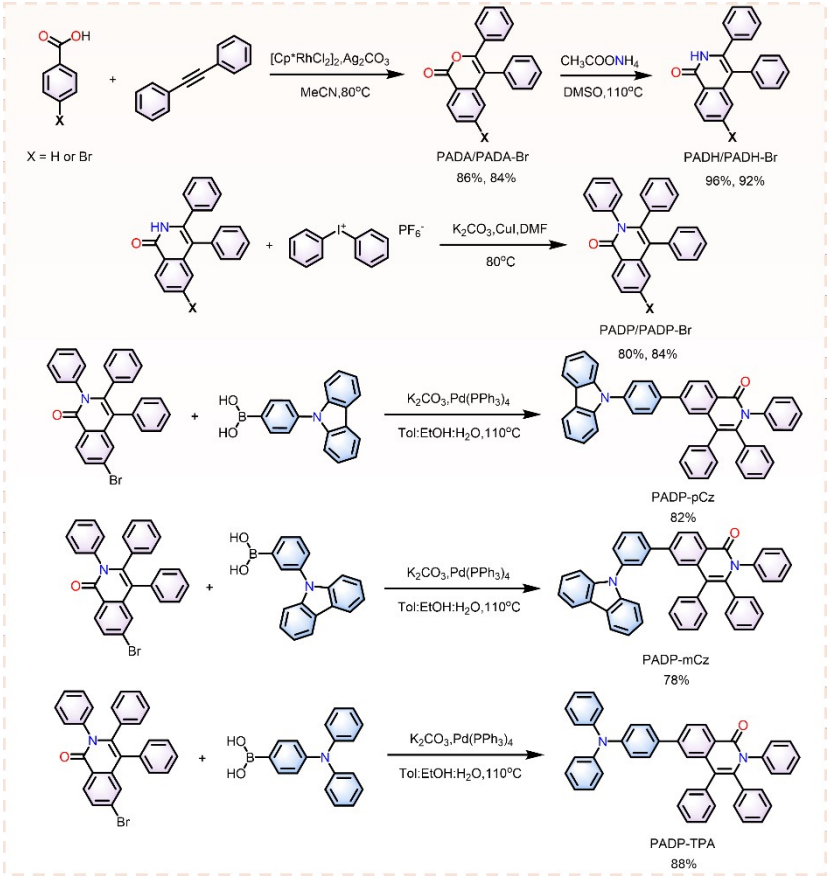

Scheme S1. Molecular structures and synthetic routes of the **PADP**, **PADP-pCz**, **PADP-mCz** and **PADP-TPA**.

3,4-diphenyl-1H-isochromen-1-one (PADA): Benzoic acid (1.0 g, 8.19 mmol), 1,2-diphenylethyne (1.75 g, 9,83 mmol), bis [(pentamethylcyclopentadienyl)dichloro-rhodium] (253.41 mg, 0.41 mmol) and silver carbonate (4.52 g, 16.39 mmol) were placed in a 250 mL round bottom flask under nitrogen. Then 80 mL of acetonitrile was injected into the bottle, and the reaction mixture was refluxed in a nitrogen atmosphere at 80 ℃ for 24 hours. After the reaction finished, cooling to room temperature. Then, the mixture was poured into the water solution and extracted with dichloromethane three times. Finally, the extract dried over anhydrous $MgSO_4$ and evaporated under reduced pressure to obtain the crude product, which was purified by silica gel column chromatograph. The white powder of PADA was obtained in 86% yield. ^{1}H NMR (500 MHz, CD_2Cl_2) δ 8.36 (d, J = 8.0 Hz, 1H), 7.66 (t, J = 7.7 Hz, 1H), 7.55 (t, J = 7.5 Hz, 1H), 7.45 – 7.39 (m, J = 3.5 Hz, 3H), 7.36 – 7.32 (m, 2H), 7.29 – 7.25 (m, 3H), 7.24 – 7.18 (m, 3H). ^{13}C NMR (101 MHz, CD_2Cl_2) δ 162.51, 151.51, 139.39, 135.16,

134.92, 133.77, 131.83, 129.81, 129.77, 129.51, 129.47, 128.66, 128.62, 128.42, 125.92, 121.05, 117.53.

3,4-diphenylisoquinolin-1(2H)-one (PADH): PADA (1 g, 3.35 mmol) and ammonium acetate (2.07 g, 26.80 mmol) were dissolved in dimethyl sulfoxide (20 mL) under a nitrogen atmosphere. Then the reaction mixture was stirred and refluxed in a nitrogen atmosphere at 110 ℃ for 12 hours. As the reaction solution cooled to room temperature, added a certain amount of deionized water to the reaction solution. Upon the addition of water, a white solid precipitated out, which can be obtained as PADH through suction filtration. The white solid of PADH was obtained in 96% yield. ^{1}H NMR (500 MHz, CD_2Cl_2) δ 9.64 (s, 1H), 8.40 (dd, J = 8.1, 1.5 Hz, 1H), 7.63 – 7.58 (m, 1H), 7.53 – 7.48 (m, 1H), 7.36 – 7.25 (m, 9H), 7.23 – 7.18 (m, 2H). ^{13}C NMR (126 MHz, CD_2Cl_2) δ 163.05, 139.34, 137.92, 136.43, 135.71, 133.18, 132.43, 130.01, 129.15, 128.87, 128.78, 127.82, 127.72, 127.08, 126.19, 125.56, 117.76.

2,3,4-triphenylisoquinolin-1(2H)-one (PADP): PADH (1 g, 3.36 mmol), diphenyliodonium hexafluorophosphate (2.15 g, 5.04 mmol), potassium carbonate (928.77 mg, 6.72 mmol) and cuprous iodide (127.60 mg, 0.67 mmol) were placed in a 100 mL round bottom flask under nitrogen. Then 30 mL N,N-dimethylformamide was injected into the bottle. Then the reaction mixture was refluxed in a nitrogen atmosphere at 80 ℃ for 24 hours. As the reaction cooled to room temperature, evaporated this reaction solution under reduced pressure. Then, the mixture was poured into the water and extracted with dichloromethane three times. Finally, the extract dried over anhydrous $MgSO_4$ and evaporated under reduced pressure to obtain the crude product, which was purified by silica gel column chromatography. The white solid of PADP was obtained in 80% yield. ^{1}H NMR (500 MHz, CD_2Cl_2) δ 8.49 (d, J = 7.9 Hz, 1H), 7.63 – 7.58 (m, 1H), 7.54 (t, J = 7.5 Hz, 1H), 7.26 – 7.20 (m, 5H), 7.19 – 7.14 (m, 4H), 7.14 – 7.11 (m, 2H), 6.97 – 6.89 (m, 5H). ^{13}C NMR (126 MHz, CD_2Cl_2) δ 141.60, 140.34, 138.34, 137.05, 135.54, 132.99, 132.29, 131.71, 130.35, 129.03, 128.50, 128.35, 127.99, 127.70, 127.59, 127.37, 126.19. HRMS ($C_{27}H_{20}NO$): m/z [M + H^+] calcd 374.1540; found: 374.1539.

6-bromo-3,4-diphenyl-1H-isochromen-1-one (PADA-Br): 4-Bromobenzoic acid (1.0 g, 4.98 mmol, Cat No.1036740, Leyan, Shanghai, China), 1,2-diphenylethyne (1.07 g, 5.98 mmol), bis [(pentamethylcyclopentadienyl)dichloro-rhodium] (154.52 mg, 0.25 mmol) and silver carbonate (2.75 g, 9.96 mmol) were placed in a 250 mL round bottom flask under nitrogen. Then 60 mL of acetonitrile was injected into the bottle, and the reaction mixture was refluxed

in a nitrogen atmosphere at 80 ℃ for 24 hours. After the reaction finished, cooling to room temperature. Then, the mixture was poured into the water solution and extracted with dichloromethane three times. Finally, the extract dried over anhydrous $MgSO_4$ and evaporated under reduced pressure to obtain the crude product, which was purified by silica gel column chromatograph. The white powder of PADA-Br was obtained in 84% yield. ^{1}H NMR (500 MHz, CD_2Cl_2) δ 8.21 (d, J = 8.4 Hz, 1H), 7.66 (dd, J = 8.4, 1.8 Hz, 1H), 7.47 – 7.41 (m, 3H), 7.34 – 7.30 (m, 3H), 7.29 – 7.24 (m, 3H), 7.24 – 7.20 (m, 2H). ^{13}C NMR (126 MHz, CD_2Cl_2) δ 161.90, 152.81, 141.00, 134.18, 133.40, 131.98, 131.73, 131.55, 130.81, 129.78, 129.74, 128.94, 128.62, 128.48, 119.78, 116.60.

6-bromo-3,4-diphenylisoquinolin-1(2H)-one (PADH-Br): PADA-Br (1 g, 2.65 mmol) and ammonium acetate (1.63 g, 21.20 mmol) were dissolved in dimethyl sulfoxide (15 mL) under a nitrogen atmosphere. Then the reaction mixture was stirred and refluxed in a nitrogen atmosphere at 110 ℃ for 12 hours. As the reaction solution cooled to room temperature, added a certain amount of deionized water to the reaction solution. Upon the addition of water, a white solid precipitated out, which can be obtained as PADH-Br through suction filtration. The white solid of PADH-Br was obtained in 92% yield. ^{1}H NMR (500 MHz, CD_2Cl_2) δ 9.32 (s, 1H), 8.27 (d, J = 8.5 Hz, 1H), 7.61 (dd, J = 8.5, 1.9 Hz, 1H), 7.46 (d, J = 1.9 Hz, 1H), 7.37 – 7.24 (m, 8H), 7.20 – 7.16 (m, 2H). ^{13}C NMR (126 MHz, CD_2Cl_2) δ 162.34, 140.91, 139.26, 135.61, 135.37, 132.30, 130.41, 129.80, 129.66, 129.45, 129.11, 128.92, 128.71, 128.64, 128.17, 124.33, 116.85.

6-bromo-2,3,4-triphenylisoquinolin-1(2H)-one (PADP-Br): PADH-Br (1 g, 2.66 mmol), diphenyliodonium hexafluorophosphate (1.70 g, 3.99 mmol), potassium carbonate (735.28 mg, 5.32 mmol) and cuprous iodide (100.91 mg, 0.53 mmol) were placed in a 100 mL round bottom flask under nitrogen. Then 25 mL N,N-dimethylformamide was injected into the bottle. Then the reaction mixture was refluxed in a nitrogen atmosphere at 80 ℃ for 24 hours. As the reaction cooled to room temperature, evaporated this reaction solution under reduced pressure. Then, the mixture was poured into the water and extracted with dichloromethane three times. Finally, the extract dried over anhydrous $MgSO_4$ and evaporated under reduced pressure to obtain the crude product, which was purified by silica gel column chromatography. The white solid of PADP-Br was obtained in 84% yield. ^{1}H NMR (400 MHz, CD_2Cl_2) δ 8.36 (d, J = 8.5 Hz, 1H), 7.63 (dd, J = 8.6, 1.9 Hz, 1H), 7.39 – 7.32 (m, 1H), 7.26 – 7.08 (m, 10H), 6.92 (s, 5H). ^{13}C

NMR (126 MHz, CD_2Cl_2) δ 143.10, 140.03, 139.91, 136.29, 135.22, 132.19, 131.53, 130.64, 130.35, 130.22, 129.11, 128.72, 128.64, 128.30, 128.17, 127.88, 127.67.

6-(4-(9H-carbazol-9-yl)phenyl)-2,3,4-triphenylisoquinolin-1(2H)-one (PADP-pCz): A mixture of compound PADP-Br (1 g, 2.21 mmol), 4-(9H-Carbozol-9-yl)phenylboronic acid (953.24 mg, 3.32 mmol), tetrakis(triphenylphosphine)palladium (150.22 mg, 0.13 mmol), and potassium carbonate (2 M) added in 250 mL round bottom flask under nitrogen. Then, a mixed solvent system of toluene, C_2H_5OH and H_2O (v/v/v = 8:1:1) was injected into the bottle, and the reaction mixture was refluxed for 24 hours. After cooling to room temperature, the mixture was poured into water and extracted three times with dichloromethane, and then dried over anhydrous $MgSO_4$. After filtration, the solvent was evaporated under reduced pressure and the residue was purified by silica gel column chromatography. The white solid of PADP-pCz was obtained in 82% yield. ^{1}H NMR (400 MHz, CD_2Cl_2) δ 8.63 (d, J = 8.3 Hz, 1H), 8.16 (d, J = 7.7 Hz, 2H), 7.89 (dd, J = 8.3, 1.8 Hz, 1H), 7.82 – 7.75 (m, 2H), 7.66 – 7.61 (m, 2H), 7.54 (d, J = 1.8 Hz, 1H), 7.47 – 7.39 (m, 4H), 7.32 – 7.23 (m, 8H), 7.22 – 7.14 (m, 4H), 7.00 – 6.92 (m, 5H). ^{13}C NMR (101 MHz, CD_2Cl_2) δ 162.82, 144.74, 142.34, 141.27, 140.37, 139.81, 138.90, 138.17, 137.00, 135.52, 132.31, 131.72, 130.33, 129.40, 129.35, 129.07, 128.64, 128.06, 127.85, 127.76, 127.65, 127.51, 126.57, 126.40, 125.30, 124.41, 123.96, 120.80, 120.62, 119.25, 110.31. HRMS ($C_{45}H_{30}N_2NaO$): m/z [M + Na^+] calcd 637.2251; found: 637.2250.

6-(3-(9H-carbazol-9-yl)phenyl)-2,3,4-triphenylisoquinolin-1(2H)-one (PADP-mCz): A mixture of compound PADP-Br (1 g, 2.21 mmol), 3-(9H-Carbazol-9-yl)phenylboronic acid (953.24 mg, 3.32 mmol), tetrakis(triphenylphosphine)palladium (150.22 mg, 0.13 mmol), and potassium carbonate (2 M) added in 250 mL round bottom flask under nitrogen. Then, a mixed solvent system of toluene, C_2H_5OH and H_2O (v/v/v = 8:1:1) was injected into the bottle, and the reaction mixture was refluxed for 24 hours. After cooling to room temperature, the mixture was poured into water and extracted three times with dichloromethane, and then dried over anhydrous $MgSO_4$. After filtration, the solvent was evaporated under reduced pressure and the residue was purified by silica gel column chromatography. The white solid of PADP-mCz was obtained in 78% yield. ^{1}H NMR (400 MHz, CD_2Cl_2) δ 8.59 (d, J = 8.3 Hz, 1H), 8.16 (dt, J = 7.9, 1.0 Hz, 2H), 7.83 (dd, J = 8.4, 1.8 Hz, 1H), 7.75 (t, J = 1.9 Hz, 1H), 7.70 – 7.57 (m, 3H), 7.50 (d, J = 1.8 Hz, 1H), 7.43 – 7.37 (m, 4H), 7.32 – 7.28 (m, 2H), 7.27 – 7.13 (m, 10H), 6.98 – 6.91 (m, 5H). ^{13}C NMR (101 MHz, CD_2Cl_2) δ 162.77, 144.83, 142.96, 142.31, 141.19, 140.33, 138.88, 138.83, 136.88, 136.86, 135.49, 135.48, 132.25, 131.70, 131.00, 130.31, 129.33,

129.07, 129.06, 128.63, 128.05, 127.76, 127.64, 127.54, 126.85, 126.65, 126.46, 126.30, 125.42, 124.75, 123.93, 120.79, 120.62, 119.22, 110.23. HRMS ($C_{45}H_{30}N_2NaO$): m/z [M + Na^+] calcd 637.2251; found: 637.2250.

6-(4-(diphenylamino)phenyl)-2,3,4-triphenylisoquinolin-1(2H)-one (PADP-TPA): A mixture of compound PADP-Br (1 g, 2.21 mmol), 4-(Diphenylamino)phenylboronic acid (959.95 mg, 3.32 mmol), tetrakis(triphenylphosphine)palladium (150.22 mg, 0.13 mmol), and potassium carbonate (2 M) added in 250 mL round bottom flask under nitrogen. Then, a mixed solvent system of toluene, C_2H_5OH and H_2O (v/v/v = 8:1:1) was injected into the bottle, and the reaction mixture was refluxed for 24 hours. After cooling to room temperature, the mixture was poured into water and extracted three times with dichloromethane, and then dried over anhydrous $MgSO_4$. After filtration, the solvent was evaporated under reduced pressure and the residue was purified by silica gel column chromatography. The white solid of PADP-TPA was obtained in 88% yield. ^1H NMR (500 MHz, CD_2Cl_2) δ 8.52 (d, J = 8.3 Hz, 1H), 7.76 (dd, J = 8.3, 1.8 Hz, 1H), 7.43 – 7.40 (m, 2H), 7.38 (d, J = 1.8 Hz, 1H), 7.29 – 7.25 (m, 4H), 7.25 – 7.12 (m, 10H), 7.11 – 7.08 (m, 4H), 7.07 – 7.04 (m, 4H), 6.97 – 6.91 (m, 5H). ^{13}C NMR (126 MHz, CD_2Cl_2) δ 162.86, 148.65, 147.98, 145.06, 142.04, 140.42, 138.81, 137.07, 135.59, 134.04, 132.28, 131.72, 130.35, 129.89, 129.08, 129.02, 128.54, 127.98, 127.69, 127.60, 127.42, 125.94, 125.29, 124.59, 123.88, 123.74, 123.52, 119.29. HRMS ($C_{45}H_{32}N_2NaO$): m/z [M + Na^+] calcd 639.2407; found: 639.2407.

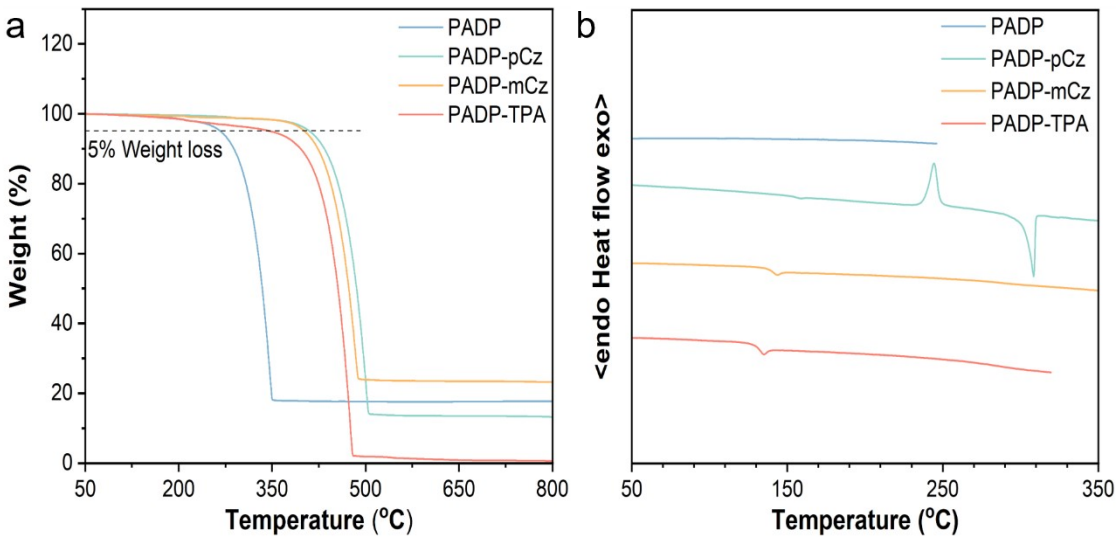

Figure S1. (a) Thermogravimetric analysis and (b) differential scanning calorimetry curve of **PADP**, **PADP-pCz**, **PADP-mCz**, and **PADP-TPA**.

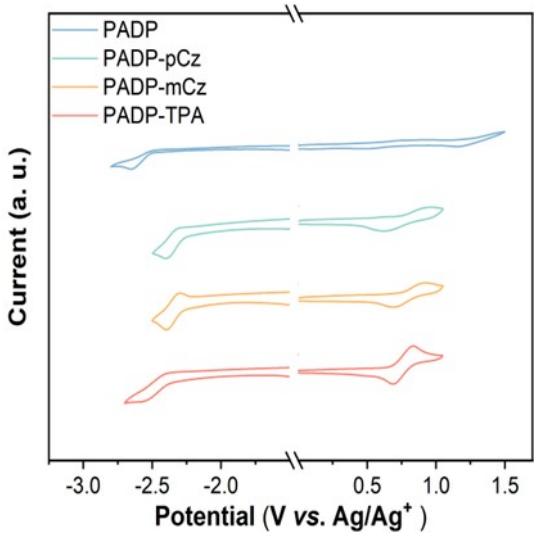

Figure S2. Cyclic voltammogram of **PADP**, **PADP-pCz**, **PADP-mCz**, and **PADP-TPA**.

S-3 X-ray Crystallography

The crystals of **PADP**, **PADP-pCz**, and **PADP-mCz** were grown from a tetrahydrofuran/methyl alcohol system via slow solvent evaporation. CCDC 2526442, 2526443, and 2526444 contain the supplementary crystallographic data for this paper.

Table S1. Crystal data and structure refinement for **PADP**.

Identification code	PADP
Empirical formula	$C_{27.5}H_{20}ClNO$
Formula weight	415.89
Temperature/K	100.00(10)
Crystal system	monoclinic
Space group	$P2_1/n$
a/Å	10.1296(2)
b/Å	19.0519(3)
c/Å	22.3359(5)
α/°	90
β/°	101.440(2)
γ/°	90
Volume/Å^3	4224.92(16)
Z	8
ρ_{calc}g/cm^3	1.308
μ/mm^{-1}	1.742
F(000)	1736.0
Crystal size/mm^3	0.14 × 0.12 × 0.1
Radiation	Cu Kα (λ = 1.54184)
2Θ range for data collection/°	8.078 to 133.198
Index ranges	$-9 \le h \le 11$, $-22 \le k \le 22$, $-26 \le l \le 26$
Reflections collected	49801
Independent reflections	7359 [R_{int} = 0.0504, R_{sigma} = 0.0296]
Data/restraints/parameters	7359/0/550
Goodness-of-fit on F^2	1.168
Final R indexes [I>=2σ (I)]	R_1 = 0.1053, wR_2 = 0.2639
Final R indexes [all data]	R_1 = 0.1133, wR_2 = 0.2680
Largest diff. peak/hole / e Å^{-3}	0.48/-0.81

Table S2. Crystal data and structure refinement for **PADP-pCz**.

Identification code	PADP-pCz
Empirical formula	$C_{45}H_{30}N_2O$
Formula weight	614.71
Temperature/K	102(3)
Crystal system	triclinic
Space group	P-1
a/Å	9.8050(6)
b/Å	18.3387(11)
c/Å	20.2686(11)
α/°	63.146(6)
β/°	80.571(5)
γ/°	83.606(6)
Volume/Å^3	3204.7(4)
Z	4
ρ_{calc}g/cm^3	1.274
μ/mm^{-1}	0.589
F(000)	1288.0
Crystal size/mm^3	0.16 × 0.1 × 0.08
Radiation	Cu Kα (λ = 1.54184)
2Θ range for data collection/°	8.784 to 133.198
Index ranges	$-11 \le h \le 11$, $-18 \le k \le 21$, $-24 \le l \le 24$
Reflections collected	44643
Independent reflections	10911 [R_{int} = 0.0999, R_{sigma} = 0.1042]
Data/restraints/parameters	10911/840/865
Goodness-of-fit on F^2	1.303
Final R indexes [I>=2σ (I)]	R_1 = 0.1796, wR_2= 0.3447
Final R indexes [all data]	R_1 = 0.2111, wR_2= 0.3608
Largest diff. peak/hole / e Å^{-3}	0.50/-0.59

Table S3. Crystal data and structure refinement for **PADP-mCz**.

Identification code	PADP-mCz
Empirical formula	$C_{45}H_{30}N_2O$
Formula weight	614.71
Temperature/K	120.00(10)
Crystal system	monoclinic
Space group	C2/c
a/Å	11.91870(10)
b/Å	19.0723(2)
c/Å	29.5542(3)
α/°	90
β/°	91.6540(10)
γ/°	90
Volume/Å^3	6715.37(11)
Z	8
ρ_{calc}g/cm3	1.216
μ/mm^{-1}	0.562
F(000)	2576.0
Crystal size/mm^3	0.15 × 0.12 × 0.1
Radiation	Cu Kα (λ = 1.54184)
2Θ range for data collection/°	5.984 to 149.958
Index ranges	$-14 \le h \le 13$, $-22 \le k \le 23$, $-35 \le l \le 36$
Reflections collected	20614
Independent reflections	6574 [R_{int} = 0.0194, R_{sigma} = 0.0174]
Data/restraints/parameters	6574/0/433
Goodness-of-fit on F^2	1.014
Final R indexes [I>=2σ (I)]	R_1 = 0.0391, wR_2 = 0.1078
Final R indexes [all data]	R_1 = 0.0410, wR_2 = 0.1097
Largest diff. peak/hole / e Å^{-3}	0.20/-0.24

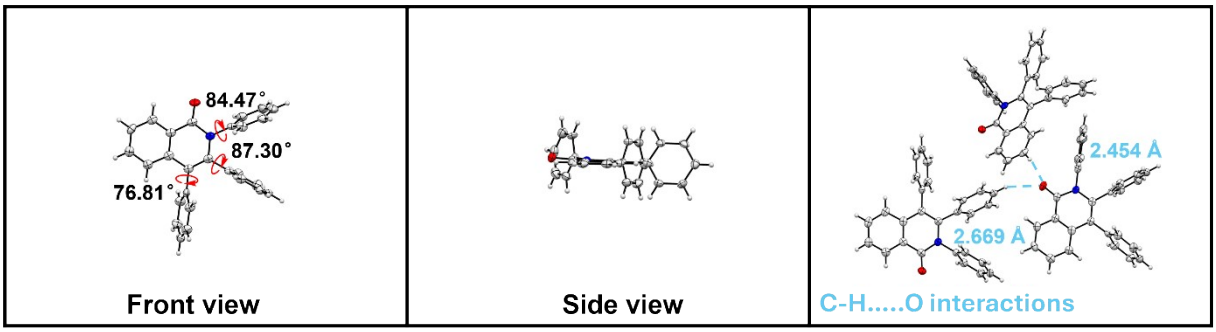

Figure S3. The ftont view, side view and hydrogen bond structure of the **PADP** crystal.

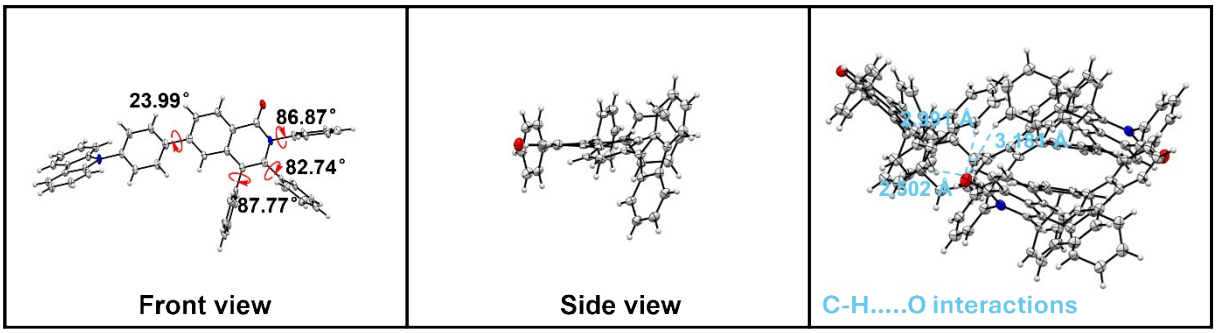

Figure S4. The ftont view, side view and hydrogen bond structure of the **PADP-pCz** crystal.

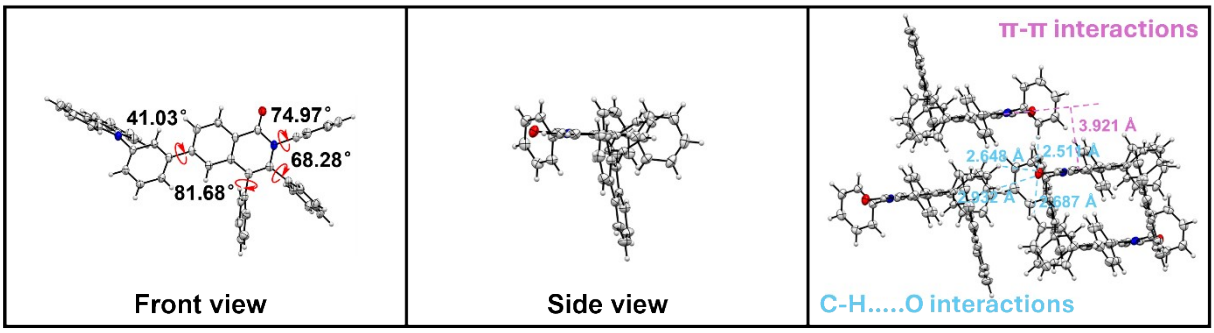

Figure S5. The front view, side view, hydrogen bonds and packing structure of the **PADP-mCz** crystal.

S-4 Computational Methods

All density functional theory (DFT) and time-dependent DFT (TD-DFT) calculations were carried out using Gaussian 16 package. The optimized structure in the gas were calculated by DFT method at the B3LYP/6–31G (d, p) level. The S_1 geometry was optimized by time-dependent DFT (TD-DFT) at the TD-M062X/6–31G (d, p) level. For better understanding of the excited-state properties, natural transition orbitals (NTO) and energy levels of the first ten singlet and triplet states were performed on the basis of S_1 geometry at the same level. To reduce computational costs within the ORCA software package, the spin-orbit mean-field (SOMF) method was combined with the RIJCOSX method to calculate SOC values. The functional and basis set employed were consistent with those used in the TD-DFT calculations.

Table S4. Cartesian coordinates for the optimized structure of ground-state (S_0) geometry of **PADP**.

Atom	x	y	z
N	1.0481348	1.02180447	0.03551416
C	0.70853855	2.39397511	0.05869163
C	-0.73011549	2.6875343	0.04161761
C	-1.69296067	1.6525391	0.00310914
C	-1.24751419	0.26806851	-0.0057798
C	0.09471925	-0.00956405	0.0189892
O	1.58169394	3.25486637	0.0780893
C	0.61060623	-1.41231758	0.0632234
C	-2.26619527	-0.82854054	0.01000917
C	-3.04799081	-1.09127117	-1.12619556
C	-4.01396964	-2.09771938	-1.11311323
C	-4.21790622	-2.85804726	0.03956679
C	-3.4522703	-2.60234624	1.1778941
C	-2.48863468	-1.59385147	1.16378042
C	1.27423128	-1.89433933	1.2012258
C	1.72882844	-3.21068359	1.251855
C	1.53198738	-4.06365802	0.16434588
C	0.87388048	-3.5930744	-0.97218734
C	0.4146026	-2.2772924	-1.02169097
C	-1.12327925	4.03601435	0.06247648
C	-2.46639804	4.3732347	0.05445208
C	-3.43321938	3.35487208	0.0313603
C	-3.05813509	2.02086587	0.00837559
C	2.46155748	0.73493793	-0.08292669
C	2.97508317	0.25859463	-1.2891063
C	4.33951523	-0.00847156	-1.40335328
C	5.19055538	0.21544422	-0.32094386
C	4.67379163	0.71100263	0.87790078
C	3.31044483	0.97298257	0.99888411

H	-2.89169106	-0.50219196	-2.02571569
H	-4.60495309	-2.28911291	-2.00430312
H	-4.96880117	-3.64265789	0.05074013
H	-3.60637769	-3.18672286	2.080485
H	-1.89660104	-1.39710196	2.05218059
H	1.43111532	-1.23531412	2.0492484
H	2.23654168	-3.57028425	2.14200539
H	1.8883304	-5.0887751	0.20377336
H	0.71548538	-4.2501141	-1.82226731
H	-0.10388421	-1.91603923	-1.90379829
H	-0.34314368	4.78876368	0.08737342
H	-2.77045513	5.41530918	0.07095226
H	-4.48880756	3.61198017	0.03451302
H	-3.81690088	1.24742368	-0.00194577
H	2.30804283	0.09701721	-2.1292042
H	4.73583914	-0.38581854	-2.34117232
H	6.25300248	0.01045531	-0.41225874
H	5.33307768	0.89757066	1.72025359
H	2.90116811	1.37071683	1.92106405

Table S5. Cartesian coordinates for the optimized structure of ground-state (S_0) geometry of **PADP-pCz**.

Atom	x	y	z
N	4.60522986	-1.27990253	-0.1139391
C	3.70170206	-2.36412907	-0.20506327
C	2.28085854	-2.00269129	-0.15678152
C	1.86299305	-0.65950154	-0.02252841
C	2.86636115	0.39059608	0.05494406
C	4.19535797	0.05844554	-0.00088143
O	4.11149948	-3.51554555	-0.30528201
C	5.26958794	1.09835886	0.02290012
C	2.42569186	1.81799495	0.14813429
C	2.53936658	2.68490954	-0.94799576
C	2.10813789	4.0087198	-0.85983764
C	1.54714118	4.48723871	0.32486505
C	1.41929862	3.63281928	1.42133411
C	1.85302445	2.30989589	1.33205018
C	5.47927655	1.87895453	1.16754575
C	6.46489596	2.86536306	1.18260299
C	7.25149291	3.0877621	0.05208206
C	7.04748619	2.31774952	-1.09440036
C	6.06592446	1.32863892	-1.1086523
C	1.33228998	-3.03417711	-0.2456531
C	-0.02008049	-2.75101083	-0.21346488
C	-0.46898956	-1.41493998	-0.09998039
C	0.47718354	-0.39358199	-0.01012352
C	6.00396564	-1.64313479	-0.03578949
C	6.68539242	-1.5272057	1.1756541
C	8.03118092	-1.88689925	1.24987363
C	8.68913694	-2.37623414	0.12128829
C	7.99641487	-2.50841918	-1.08389355
C	6.65371164	-2.14418122	-1.16461439
C	-1.92006901	-1.10386242	-0.08118087
C	-2.82973121	-1.83966013	-0.8595038
C	-4.18948881	-1.54417151	-0.85584672
C	-4.68344263	-0.50975539	-0.05120329
C	-3.79122152	0.22631917	0.73879198
C	-2.43079686	-0.06372939	0.7138667
N	-6.07022593	-0.21092866	-0.03613129
C	-6.64058285	1.04547998	-0.27720387
C	-7.10277563	-1.12134659	0.22284942
C	-6.02130863	2.25265167	-0.61296121
C	-6.83637817	3.36270574	-0.8231848
C	-8.23437599	3.27823988	-0.70902801
C	-8.84622305	2.07017416	-0.38857469
C	-8.05087171	0.93889627	-0.17274958
C	-8.34540505	-0.44210363	0.1478567
C	-9.53180218	-1.14554762	0.38580592
C	-9.46606307	-2.49981263	0.69893328

C	-8.22529208	-3.15391872	0.78384805
C	-7.02963201	-2.47792841	0.55113119
H	2.97347841	2.31642474	-1.87225018
H	2.20856106	4.6656087	-1.71903915
H	1.2110288	5.51770376	0.39325985
H	0.98510391	3.99656952	2.34832495
H	1.75425002	1.6482178	2.18833412
H	4.86372165	1.71311392	2.0456346
H	6.61618043	3.46058163	2.07826279
H	8.01798191	3.85699801	0.0630576
H	7.65277791	2.48730329	-1.97999081
H	5.9125246	0.73210212	-2.00233394
H	1.6977593	-4.05148897	-0.33193474
H	-0.74287618	-3.5595622	-0.25236612
H	0.14338149	0.63564321	0.03991057
H	6.16349564	-1.1555975	2.05105983
H	8.56157565	-1.789387	2.19225791
H	9.7357844	-2.65913534	0.18130478
H	8.50048113	-2.89891741	-1.96275923
H	6.10306403	-2.25535338	-2.09230136
H	-2.46295467	-2.62835813	-1.50885199
H	-4.87203022	-2.09876404	-1.49102368
H	-4.17229181	1.00980177	1.3851803
H	-1.75763854	0.50201034	1.35014654
H	-4.94412418	2.32442431	-0.71345074
H	-6.37800029	4.31213352	-1.08393126
H	-8.84044735	4.16304512	-0.87744616
H	-9.92767783	2.00328657	-0.31120331
H	-10.49077788	-0.63823505	0.33095395
H	-10.3793748	-3.056654	0.88421331
H	-8.193917	-4.20905514	1.03913783
H	-6.07611964	-2.98810428	0.62902654

Table S6. Cartesian coordinates for the optimized structure of ground-state (S_0) geometry of **PADP-mCz**.

Atom	x	y	z
N	3.97725717	-1.44696884	-0.11591226
C	2.82934027	-2.25425188	0.05850597
C	1.58314028	-1.52520654	0.3192966
C	1.55337734	-0.11456012	0.39540439
C	2.7849837	0.63252965	0.19473831
C	3.94949605	-0.04410308	-0.0616976
O	2.90721202	-3.47656168	0.00074683
C	5.23524396	0.67174482	-0.32707174
C	2.74682706	2.12848829	0.22662456
C	2.8582984	2.88174058	-0.95070767
C	2.80197768	4.27520922	-0.91549711
C	2.62449308	4.94049978	0.29821813
C	2.50279249	4.20303767	1.47717309
C	2.56151789	2.80969158	1.44034651
C	5.85578934	1.41842181	0.68331678
C	7.04214859	2.1062263	0.43001737
C	7.6219972	2.06047608	-0.83803555
C	7.00914243	1.32235963	-1.85221214
C	5.82613187	0.63085422	-1.59859295
C	0.40583285	-2.269591	0.4956368
C	-0.79813999	-1.63488184	0.73646196
C	-0.86236558	-0.22419071	0.80063798
C	0.30969522	0.5114554	0.62582446
C	5.22595373	-2.16600156	-0.25178531
C	6.13623201	-2.18361262	0.80483027
C	7.33465052	-2.885532	0.67408363
C	7.61486289	-3.5809213	-0.50235863
C	6.69096249	-3.57561137	-1.54933709
C	5.49531951	-2.87045322	-1.42591295
C	-2.21838883	1.63780438	1.81597768
C	-3.43473589	2.28174933	2.03242461
C	-4.61545244	1.76685569	1.49961611
C	-4.56867489	0.60218146	0.72429184
C	-3.34627477	-0.03771929	0.49690228
C	-2.15630425	0.46429345	1.04576412
N	-5.76045732	0.07338086	0.15942519
C	-6.24787227	-1.22594438	0.34365423
C	-6.64489697	0.76184479	-0.67940026
C	-5.73178792	-2.26590128	1.12170771
C	-6.43521594	-3.46804142	1.14591877
C	-7.62673546	-3.63480618	0.41971935
C	-8.14322483	-2.59108654	-0.34204973
C	-7.45678595	-1.37192426	-0.38350866
C	-7.70904522	-0.10481009	-1.03739779
C	-8.71920003	0.35888381	-1.88815395
C	-8.65396555	1.66234791	-2.37106316

C	-7.58504211	2.50307184	-2.01685264
C	-6.56695144	2.06755462	-1.17161322
H	2.99442615	2.36820686	-1.89738422
H	2.89425017	4.84086001	-1.8381689
H	2.580151	6.02530725	0.32543305
H	2.36580031	4.71209351	2.42705155
H	2.46902016	2.23880467	2.36031766
H	5.4027309	1.46186485	1.66836247
H	7.51167105	2.67892833	1.22433659
H	8.54495218	2.59744144	-1.03595299
H	7.45187926	1.28491867	-2.84315517
H	5.35459472	0.05760809	-2.3904932
H	0.47751958	-3.35029916	0.44259607
H	-1.69620109	-2.2226336	0.8969537
H	0.26350877	1.59355896	0.63630219
H	5.90587628	-1.64885336	1.72014586
H	8.04499673	-2.89230921	1.49523032
H	8.54655056	-4.12977543	-0.6014487
H	6.89889549	-4.12400617	-2.46311277
H	4.76515018	-2.8708608	-2.22783014
H	-1.31250784	2.03196914	2.26473586
H	-3.46794792	3.18072971	2.64057478
H	-5.56900215	2.2485689	1.68717129
H	-3.32412052	-0.91348725	-0.1423661
H	-4.81930303	-2.14092531	1.69413717
H	-6.05325405	-4.29148018	1.74217481
H	-8.14922835	-4.58561021	0.45842658
H	-9.06971572	-2.71807584	-0.89478783
H	-9.54088255	-0.29314779	-2.17050288
H	-9.43209614	2.03376109	-3.03071952
H	-7.54733305	3.51425669	-2.41134162
H	-5.74055581	2.71916575	-0.91032314

Table S7. Cartesian coordinates for the optimized structure of ground-state (S_0) geometry of **PADP-TPA**.

Atom	x	y	z
N	4.55970928	-1.2384986	-0.23918964
C	3.65542974	-2.30107167	-0.47410171
C	2.23571332	-1.94050225	-0.41787366
C	1.81662574	-0.61747785	-0.15062367
C	2.82066658	0.40768787	0.09036467
C	4.14953031	0.07363633	0.04874215
O	4.0666907	-3.43088434	-0.71706615
C	5.22386576	1.07249854	0.33895915
C	2.38055515	1.79866692	0.42463179
C	2.49602308	2.30262467	1.72796488
C	2.06599206	3.59352304	2.03595469
C	1.50417062	4.40145063	1.04664641
C	1.3743011	3.90955912	-0.25326847
C	1.80701265	2.61926481	-0.5598723
C	6.02008374	0.95176755	1.48753092
C	7.00217396	1.898762	1.77160015
C	7.20700963	2.97786462	0.90987718
C	6.4206244	3.10602119	-0.23531953
C	5.43470914	2.16111115	-0.51783889
C	1.28599978	-2.95057729	-0.64175055
C	-0.06589313	-2.66853347	-0.59547401
C	-0.51749744	-1.35842354	-0.31048791
C	0.43128558	-0.35853888	-0.08899174
C	5.95777233	-1.56154338	-0.42388591
C	6.60817646	-2.38047966	0.50027589
C	7.95071005	-2.70359843	0.31271971
C	8.64326336	-2.21352427	-0.79636829
C	7.98498115	-1.40590145	-1.72395698
C	6.63927896	-1.08539149	-1.54393892
C	-1.96766302	-1.05500458	-0.24603587
C	-2.88837931	-1.99265372	0.25241345
C	-4.24966276	-1.71734773	0.31016124
C	-4.74690067	-0.47587018	-0.12002331
C	-3.83503435	0.47210296	-0.61374698
C	-2.47770661	0.18066233	-0.6802053
N	-6.13338699	-0.18710781	-0.05808374
C	-6.75858001	0.54764017	-1.10390043
C	-6.90780948	-0.63246721	1.04951632
C	-7.6885531	1.55645654	-0.80642107
C	-8.30833274	2.26545694	-1.83333277
C	-8.00104226	1.99657217	-3.16851449
C	-7.07017112	0.99955045	-3.46688324
C	-6.4589116	0.27224967	-2.44769944
C	-6.41123976	-0.52126782	2.35808518
C	-7.17180135	-0.96515716	3.43784031
C	-8.4426111	-1.50748127	3.2366036

C	-8.94279938	-1.60986447	1.93708349
C	-8.1822896	-1.18607392	0.84922749
H	2.93065701	1.6768553	2.50125321
H	2.16783282	3.96669861	3.05097872
H	1.16858838	5.40611547	1.28665251
H	0.93881505	4.53119595	-1.03051037
H	1.70601179	2.24020168	-1.57319228
H	5.86606623	0.11416521	2.16041829
H	7.60723729	1.79376001	2.66733785
H	7.97387753	3.71440028	1.13087999
H	6.57240667	3.942966	-0.9105479
H	4.8193158	2.26726508	-1.40522701
H	1.6506178	-3.9485485	-0.85889197
H	-0.7879346	-3.45206572	-0.80142947
H	0.09791374	0.63972202	0.16681915
H	6.05768634	-2.76677888	1.35105484
H	8.45490224	-3.34161647	1.03228705
H	9.68985483	-2.46522971	-0.93943623
H	8.51503583	-1.02818281	-2.59307541
H	6.11716792	-0.46665994	-2.26601404
H	-2.53269104	-2.9525424	0.61414209
H	-4.9358071	-2.46264054	0.69742348
H	-4.19805164	1.43603715	-0.95328158
H	-1.80048185	0.92541602	-1.08677694
H	-7.9206251	1.77766252	0.2299067
H	-9.02563568	3.04260963	-1.58533158
H	-8.48078869	2.55592822	-3.96566381
H	-6.82682769	0.77332447	-4.50108979
H	-5.7472925	-0.51138663	-2.6850314
H	-5.43032676	-0.08739467	2.5205472
H	-6.77232434	-0.87192704	4.44366675
H	-9.03511626	-1.84553966	4.08107185
H	-9.92696238	-2.03590265	1.76421574
H	-8.56935921	-1.27985619	-0.15981208

Table S8. The natural transition orbits distribution of **PADP**.

PADP	Hole	Transition character	Particle
S_1	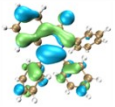	HLCT 98.5%	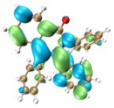
T_1	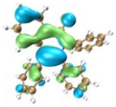	HLCT 98.8%	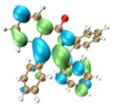
T_2	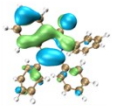	HLCT 95.4%	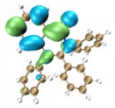
T_3	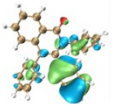	HLCT 67.1%	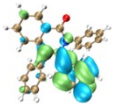
T_4	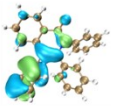	HLCT 58.5%	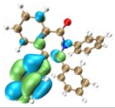

Table S9. The natural transition orbits distribution of **PADP-pCz**.

PADP-pCz	Hole	Transition character	Particle
S_1	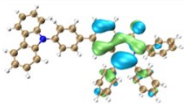	HLCT 97.0%	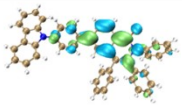
T_1	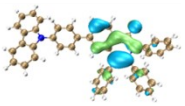	HLCT 97.0%	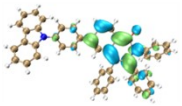
T_2	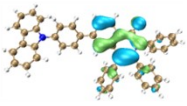	LE 95.1%	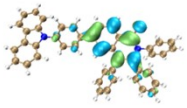
T_3	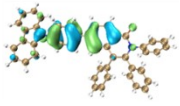	LE 67.1%	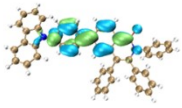
T_4	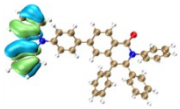	LE 82.8%	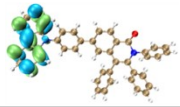

Table S10. The natural transition orbits distribution of **PADP-mCz**.

PADP-mCz	Hole	Transition character	Particle
S_1	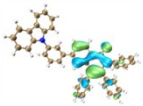	HLCT 97.1%	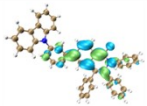
T_1	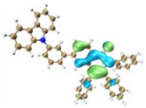	HLCT 97.2%	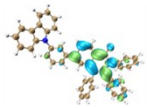
T_2	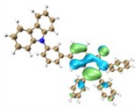	LE 95.3%	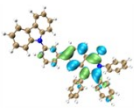
T_3	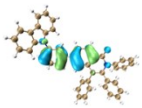	LE 87.7%	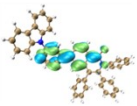
T_4	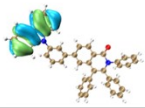	LE 82.9%	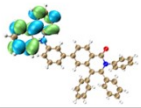

Table S11. The natural transition orbits distribution of **PADP-TPA**.

PADP-TPA	Hole	Transition character	Particle
S_1	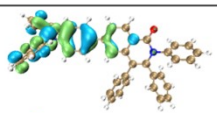	HLCT 97.2%	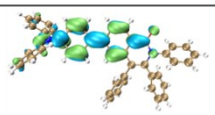
T_1	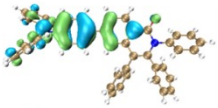	HLCT 93.6%	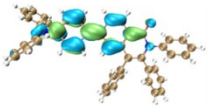
T_2	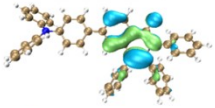	HLCT 92.6%	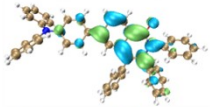
T_3	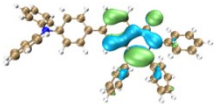	LE 93.1%	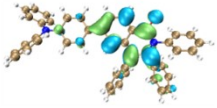
T_4	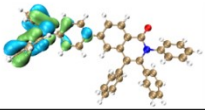	LE 87.2%	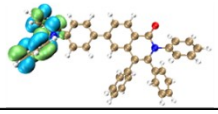

S-5 Additional Spectra and Data

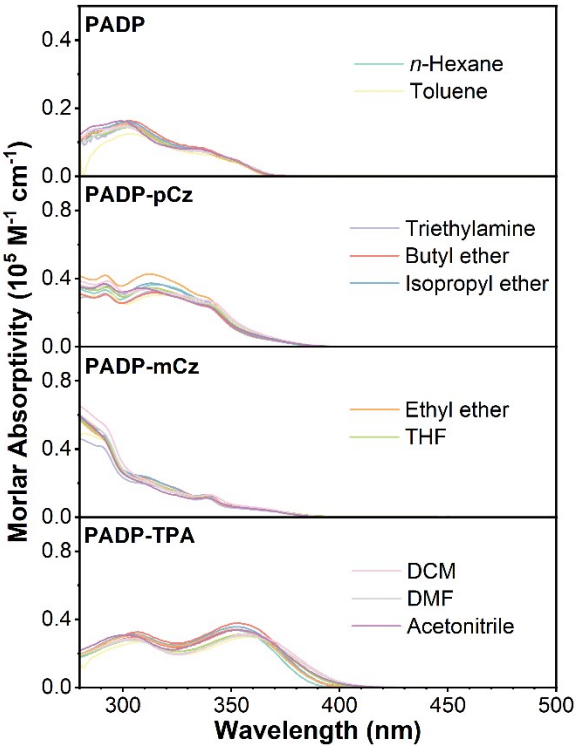

Figure S6. UV-vis absorption spectra of **PADP**, **PADP-pCz**, **PADP-mCz**, and **PADP-TPA** in solvents of different polarities.

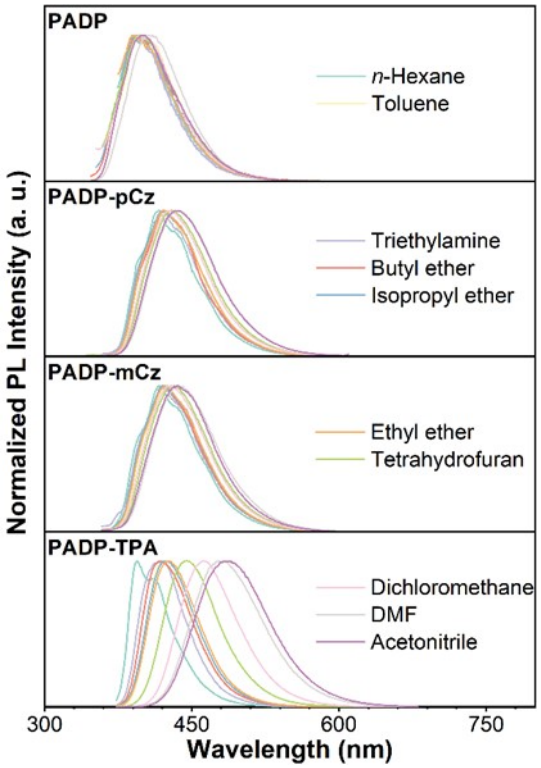

Figure S7. PL spectra of **PADP**, **PADP-pCz**, **PADP-mCz**, and **PADP-TPA** in solvents of different polarities.

Table S12. Detailed parameters of photophysical properties of **PADP**.

Solvents	ε	n	$f(\varepsilon,n)$	λ_{abs} [nm]	λ_{em} [nm]	ν_a-ν_f [cm^{-1}]
Hexane	1.9	1.375	0.0012	302	390	7471.56
Toluene	2.4	1.497	0.013	304	396	7642.21
Triethylamine	2.42	1.401	0.048	302	396	7405.64
Butyl ether	3.08	1.399	0.096	302	394	7731.87
Isopropyl ether	3.88	1.368	0.145	302	391	7537.14
Ethyl ether	4.34	1.352	0.167	302	391	7537.14
Tetrahydrofuran	7.58	1.407	0.21	302	396	7860.06
Dichloromethane	8.93	1.424	0.217	300	398	8207.71
Dimethyl formamide	37	1.427	0.276	302	406	8482.04
Acetonitrile	37.5	1.344	0.305	299	402	8569.19

Table S13. Detailed parameters of photophysical properties of **PADP-pCz**.

Solvents	ε	n	$f(\varepsilon,n)$	λ_{abs} [nm]	λ_{em} [nm]	ν_a-ν_f [cm^{-1}]
Hexane	1.9	1.375	0.0012	315	416	7707.57
Toluene	2.4	1.497	0.013	315	423	8105.37
Triethylamine	2.42	1.401	0.048	314	420	8037.61
Butyl ether	3.08	1.399	0.096	313	423	8308.22
Isopropyl ether	3.88	1.368	0.145	312	421	8298.31
Ethyl ether	4.34	1.352	0.167	312	422	8354.60
Tetrahydrofuran	7.58	1.407	0.21	313	430	8693.07
Dichloromethane	8.93	1.424	0.217	310	427	8838.86
Dimethyl formamide	37	1.427	0.276	311	438	9323.29
Acetonitrile	37.5	1.344	0.305	308	436	9531.75

Table S14. Detailed parameters of photophysical properties of **PADP-mCz**.

Solvents	ε	n	$f(\varepsilon,n)$	λ_{abs} [nm]	λ_{em} [nm]	ν_a-ν_f [cm^{-1}]
Hexane	1.9	1.375	0.0012	338	417	5604.98
Toluene	2.4	1.497	0.013	340	423	5771.10
Triethylamine	2.42	1.401	0.048	338	419	5719.45
Butyl ether	3.08	1.399	0.096	338	420	5776.28
Isopropyl ether	3.88	1.368	0.145	338	421	5832.83
Ethyl ether	4.34	1.352	0.167	338	425	6056.39
Tetrahydrofuran	7.58	1.407	0.21	339	429	6188.50
Dichloromethane	8.93	1.424	0.217	339	429	6188.50
Dimethyl formamide	37	1.427	0.276	339	437	6615.23
Acetonitrile	37.5	1.344	0.305	338	435	6597.29

Table S15. Detailed parameters of photophysical properties of **PADP-TPA**.

Solvents	ε	n	$f(\varepsilon,n)$	λ_{abs} [nm]	λ_{em} [nm]	ν_a-ν_f [cm^{-1}]
Hexane	1.9	1.375	0.0012	351	394	3109.32
Toluene	2.4	1.497	0.013	358	420	4123.44
Triethylamine	2.42	1.401	0.048	353	416	4290.15
Butyl ether	3.08	1.399	0.096	352	417	4428.28
Isopropyl ether	3.88	1.368	0.145	352	423	4768.43
Ethyl ether	4.34	1.352	0.167	353	427	4909.41
Tetrahydrofuran	7.58	1.407	0.21	356	444	5567.37
Dichloromethane	8.93	1.424	0.217	357	462	6366.18
Dimethyl formamide	37	1.427	0.276	356	477	7125.53
Acetonitrile	37.5	1.344	0.305	353	489	7878.71

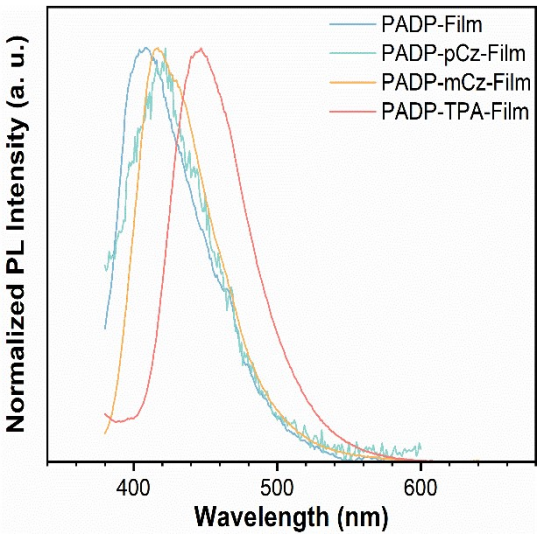

Figure S8. Vacuum-deposited neat film data of **PADP**, **PADP-pCz**, **PADP-mCz**, and **PADP-TPA**.

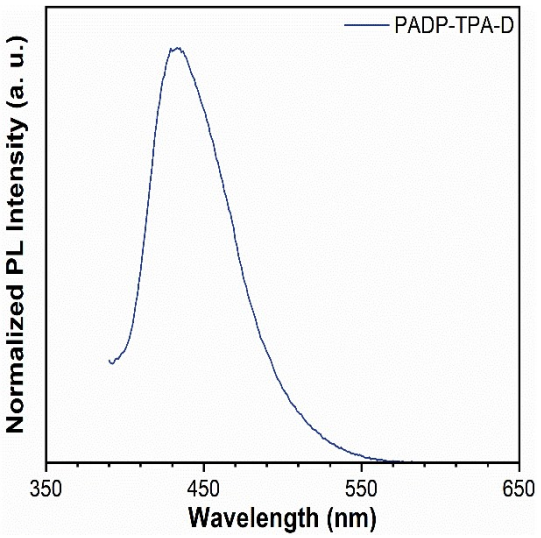

Figure S9. Vacuum-deposited doped film data of **PADP-TPA**.

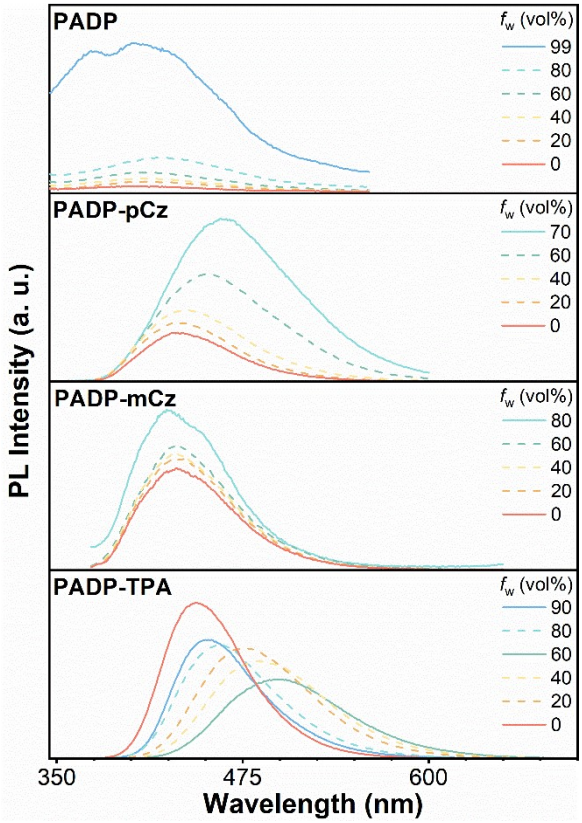

Figure S10. PL spectra in THF/water mixtures (10^{-5} M) with different water fractions (f_w).

The Lippert-Mataga model

The Lippert-Mataga model is estimated according to Equation S1

$$hc(v_a - v_f) = hc(v_a^0 - v_f^0) + \frac{2(\mu_e - \mu_g)^2}{a_0^3} f(\varepsilon,n) \quad \text{S1}$$

or

$$\mu_e = \mu_g + \{\frac{hca_0^3}{2} \cdot \left[\frac{d(v_a - v_f)}{df(\varepsilon,n)}\right]\}^{1/2} \quad \text{S2}$$

where μ_e is the dipole moment of excited state, μ_g is the dipole moment of ground state, h is the Plank constant, c is the light speed in vacuum, a_0 is the solvent Onsager cavity radius, $v_a - v_f$ is the Stokes shift, $f(\varepsilon,n)$ is the orientational polarizability of solvents and $f(\varepsilon,n) = [\frac{\varepsilon - 1}{2\varepsilon + 1} - \frac{n^2 - 1}{2n^2 + 1}]$. ε is the solvent dielectric constant and n is the solvent refractive index. μ_g was estimated by DFT (values: 3.72, 4.15, 5.16 and 3.81 D). The differential $\frac{d(v_a - v_f)}{df(\varepsilon,n)}$ can be estimated based on the solvatochromic experiment data.

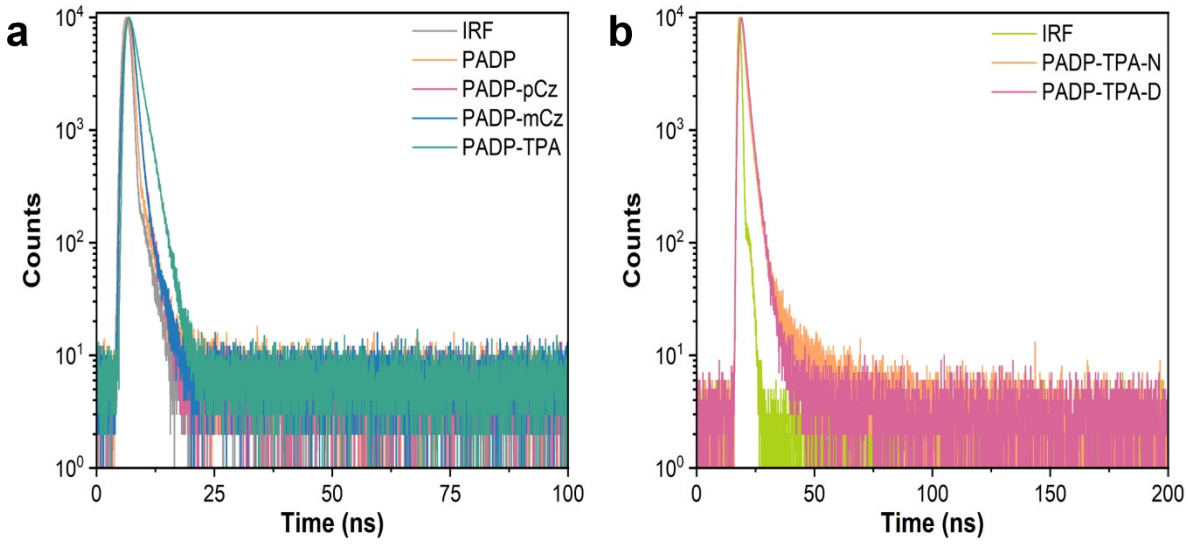

Figure S11. (a) Transient PL decay curve of **PADP**, **PADP-pCz**, **PADP-mCz** and **PADP-TPA** in 10^{-5} M toluene solution at room temperature. (b) Transient PL decay curves of pure **PADP-TPA** films and 20 wt% doped in mCPBC films at room temperature.

Table S16. Detailed parameters of photophysical properties of **PADP-TPA**.

	PADP-TPA		
	τ_F [a] [ns]	k_r [b] [10^8 S^{-1}]	k_{nr} [c] [10^8 S^{-1}]
TOL	1.75	3.98	1.74
Neat Film	2.29	2.87	1.49
Doped Film	2.18	3.72	0.87

[a] Lifetime of the prompt and delayed fluorescence. [b] k_r: Radiative transition rate. [c] k_{nr}: Non-radiative transition rate.

The values of k_r and k_{nr} for molecules in different states can be calculated using the following formula:

$$k_r = PLQY/\tau_F \quad \text{S3}$$

$$k_{nr} = (1 - PLQY)/\tau_F \quad \text{S4}$$

Calculations of radiative and non-radiative transitions for PADP-TPA in solution and thin films reveal a significant decrease in non-radiative transition rates from solution to solid state. This is attributed to aggregation-induced restriction of intramolecular motion, which substantially reduces the non-radiative transition rate.

S-6 Device Fabrication

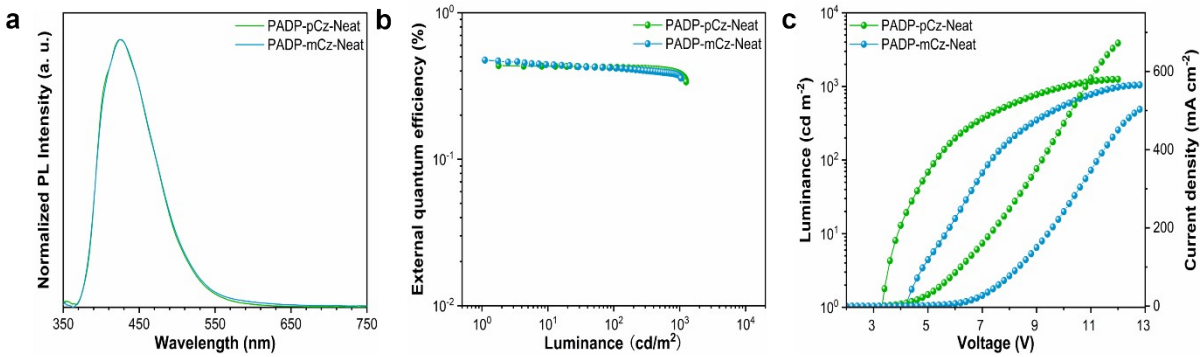

Figure S12. (a) EL emission spectrum of the neat film devices. (b) The maximum external quantum efficiency of the neat film devices. (c) Current density–voltage-luminance characteristics of the devices.

Table S17. EQE_{max}-λ_{EL} summary data of deep-blue ($\lambda_{EL} \leq 450$ nm) AIE fluorescent materials applied to OLEDs.

Emitter	λ_{EL} (nm)	EQE_{max} (%)	Reference
PADP-TPA	428	9.20	This work
TPETPAPI	444	3.80	[1]
*o*TPE-*m*TPE	435	1.40	[2]
Py-4*m*TPE	436	2.50	[3]
4,4-BtPE-PI	448	2.80	[4]
TPBS-F	438	3.60	[5]
TPP-PhCz	436	1.49	[6]
TrPP-3C	428	2.62	[7]
DPP-DPhC	424	5.73	[8]
TPB-AC	448	7.00	[9]
TPBCzC2	423	4.78	[10]
TPB-PAPC	450	6.00	[11]
CN-TPB-TPA	448	7.27	[12]
TPEA	445	8.00	[13]
1	444	2.46	[14]
TPA-3TPP	436	1.72	[15]
*m*TPE-2*m*TPE	449	1.30	[16]
DPVBi	442	2.30	[17]

BTPE-PI	450	4.00	[18]
Si-*m*TPE	432	1.21	[19]
TPA–CN–TPA	428	3.98	[20]
2TPA-CN	445	0.66	[21]
2TriPE-CzMCN	430	8.84	[22]

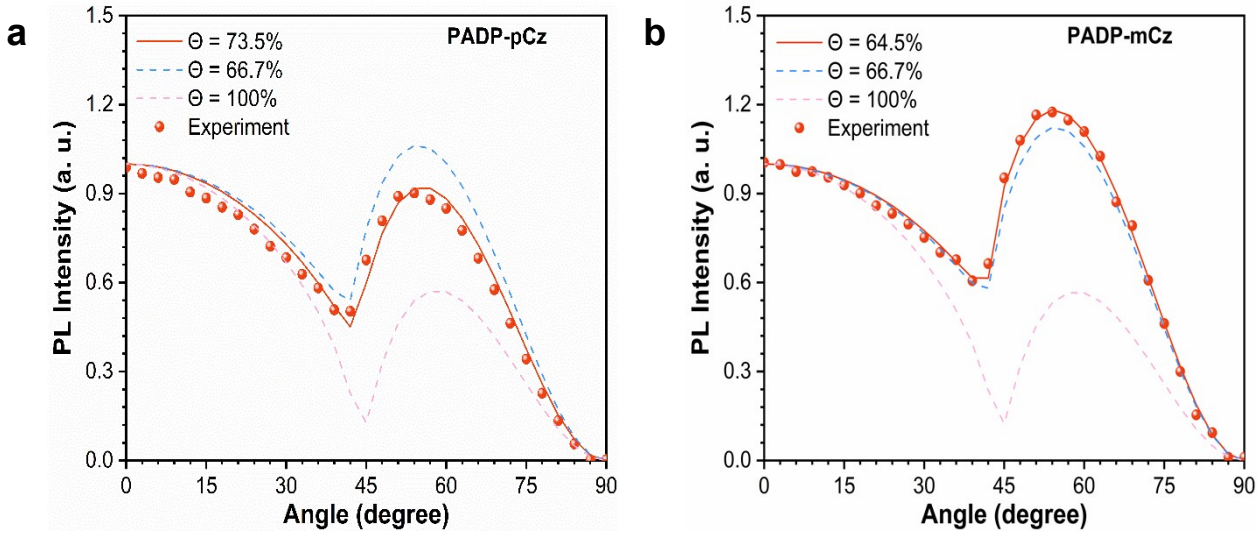

Figure S13. Measured the angle-dependent p-polarized PL spectra of a) PADP-pCz and b) PADP-mCz in neat film.

Angle-dependent PL measurements illustrate that the horizontal dipole orientation ratios (Θ//) of PADP-pCz and PADP-mCz nondoped device are 73.5% and 64.5%. Further optical simulations were performed based on the device structure, yielding η_{out} values of 27.60% and 25.20%.

Table S18. Summary of vacuum evaporation film data for the EML.

EML	η_{out}	EQE_e	EQE
PADP-pCz	0.276	0.5	0.4
PADP-mCz	0.252	0.5	0.5
PADP-TPA	0.364	6.0	6.7
MCPBC: 20 wt% PDPA-TPA	0.356	7.2	9.2

η_{out}: The light outcoupling efficiency; EQE_e: The maximum exciton utilization efficiency of conventional fluorescent materials is 25%, which is adopted as the reference value for calculations; EQE: Experimental measured values.

The calculation of EQE_e is based on Equation 1 in the main text. γ denotes the electron-hole recombination efficiency, which is set to 100% herein; η_{PL} represents the quantum yield (QY) of the vacuum-evaporated films; η_r signifies the radiative exciton utilization efficiency, with a value at 25%; and η_{out} stands for the light outcoupling efficiency.

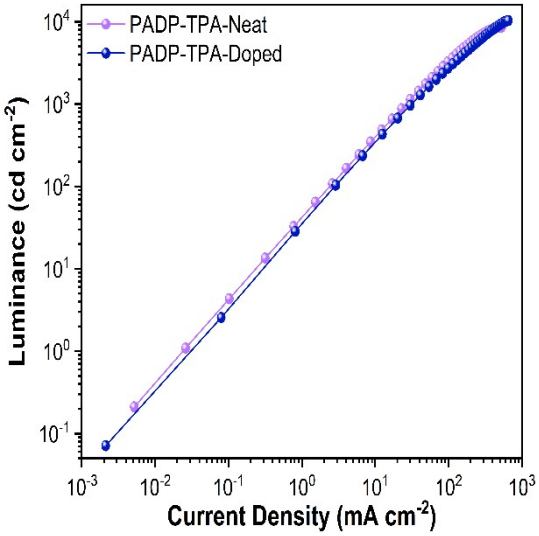

Figure S14. Current density-luminance plots.

Calculations indicate that both the pure and doped films of PADP-TPA exhibit an exciton utilization rate exceeding 25%, demonstrating that the existence of triplet-to-singlet exciton conversion in the electroluminescence, as shown in Figure S14. Below a current density of 100 mA cm^{-2}, the device exhibits a good linear relationship between current density and electroluminescence brightness, indicating that the maximum external quantum efficiency of the device does not originate from the contribution of the TTA mechanism.

S-7 NMR Spectroscopies and Mass spectrums

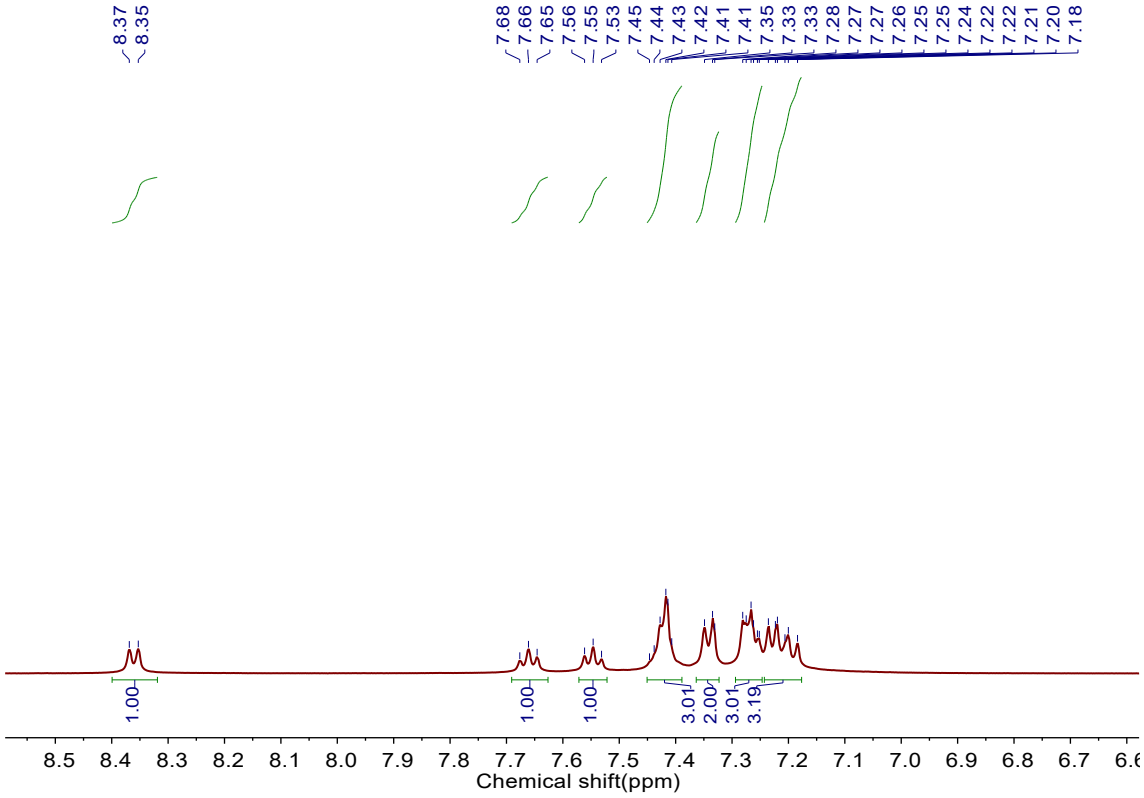

Figure S15. The ^{1}H NMR spectra of PADA in CH_2Cl_2.

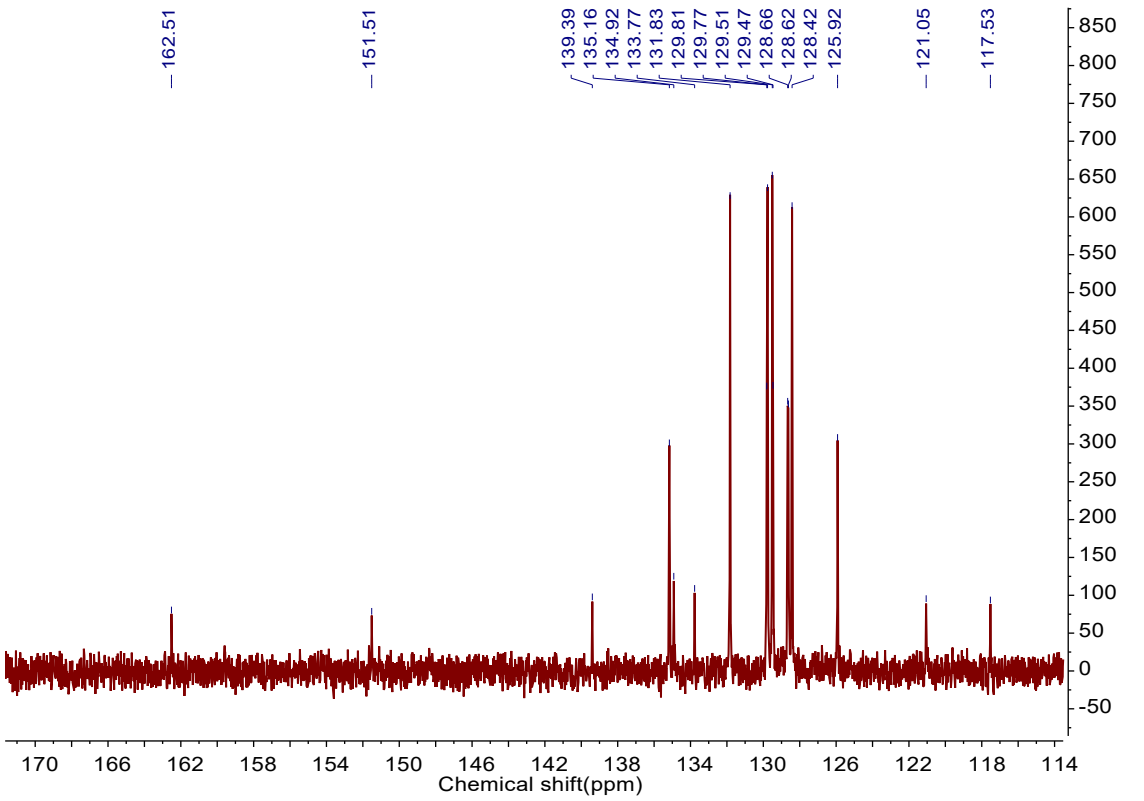

Figure S16. The ^{13}C NMR spectra of PADP in CD_2Cl_2.

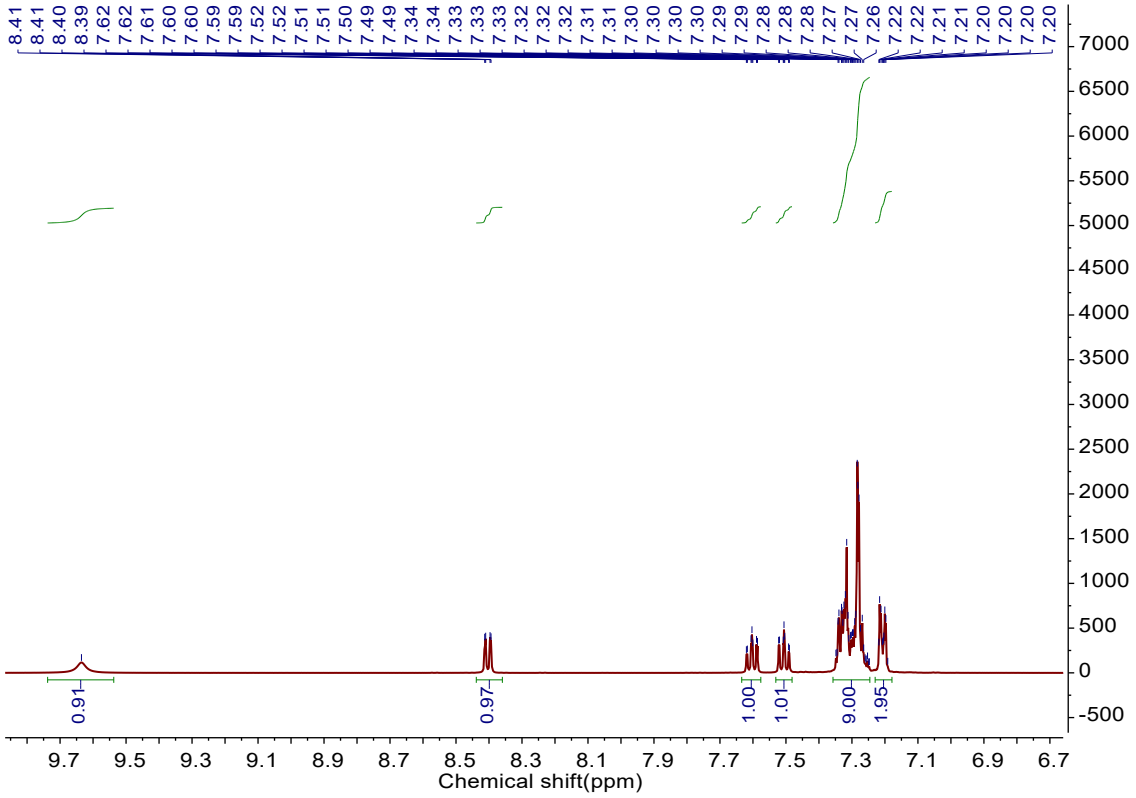

Figure S17. The ^{1}H NMR spectra of PADH in CD_2Cl_2.

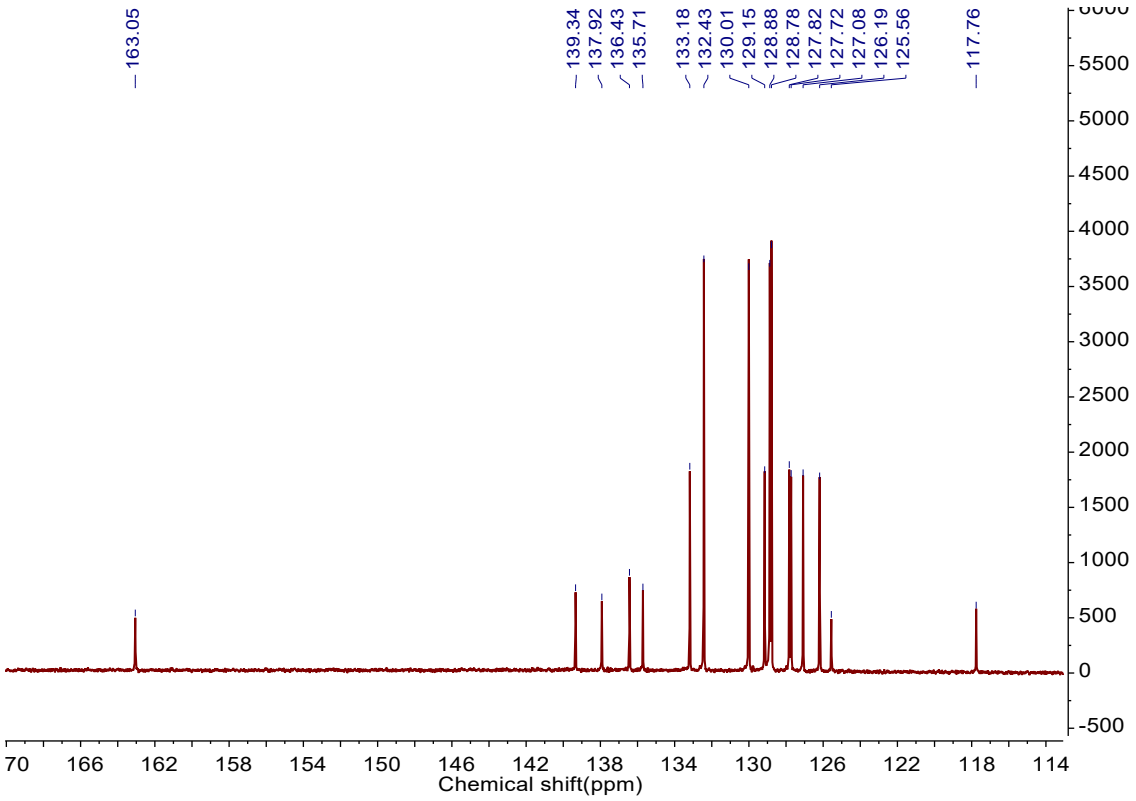

Figure S18. The ^{13}C NMR spectra of PADH in CD_2Cl_2.

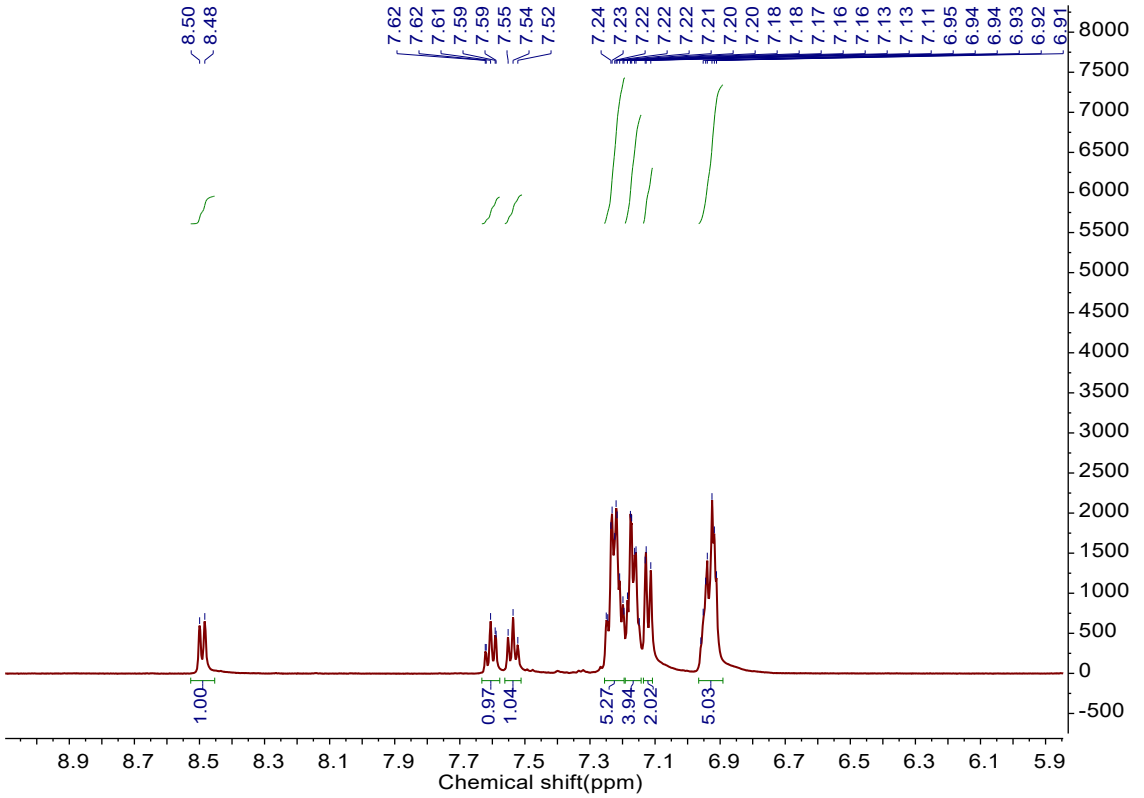

Figure S19. The ^{1}H NMR spectra of PADP in CD_2Cl_2.

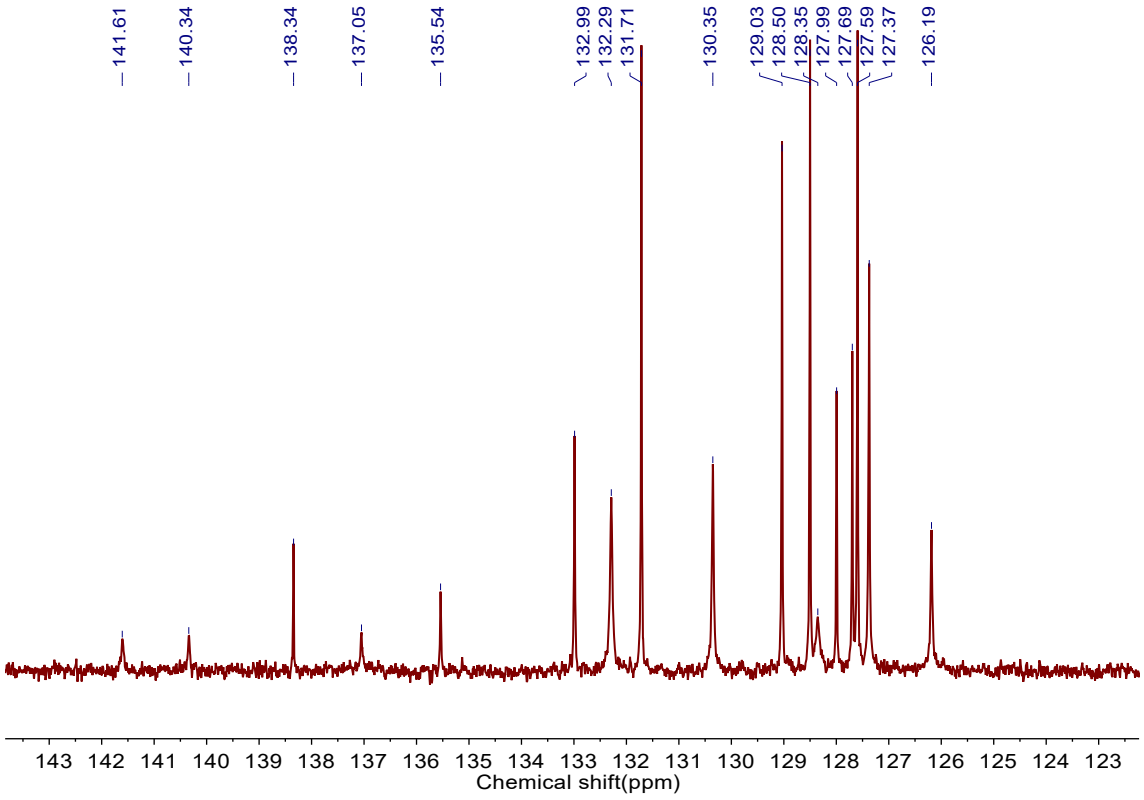

Figure S20. The ^{13}C NMR spectra of PADP in CD_2Cl_2.

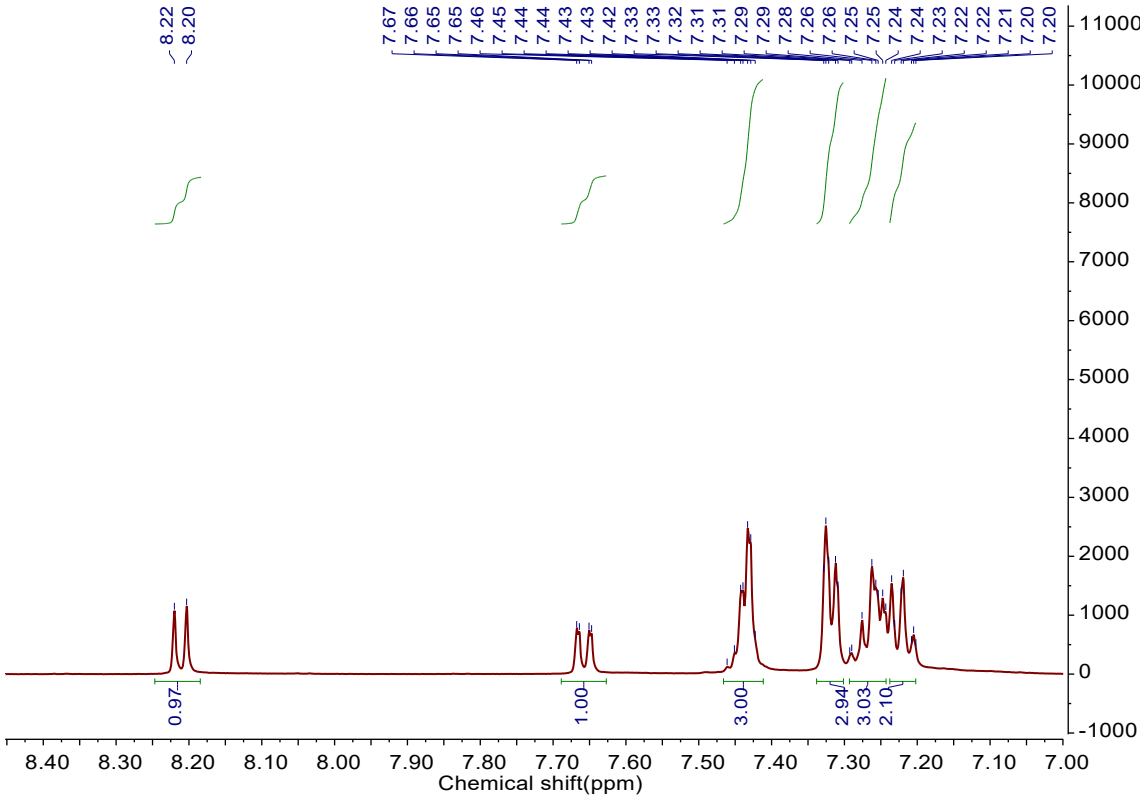

Figure S21. The ^{1}H NMR spectra of PADA-Br in CD_2Cl_2.

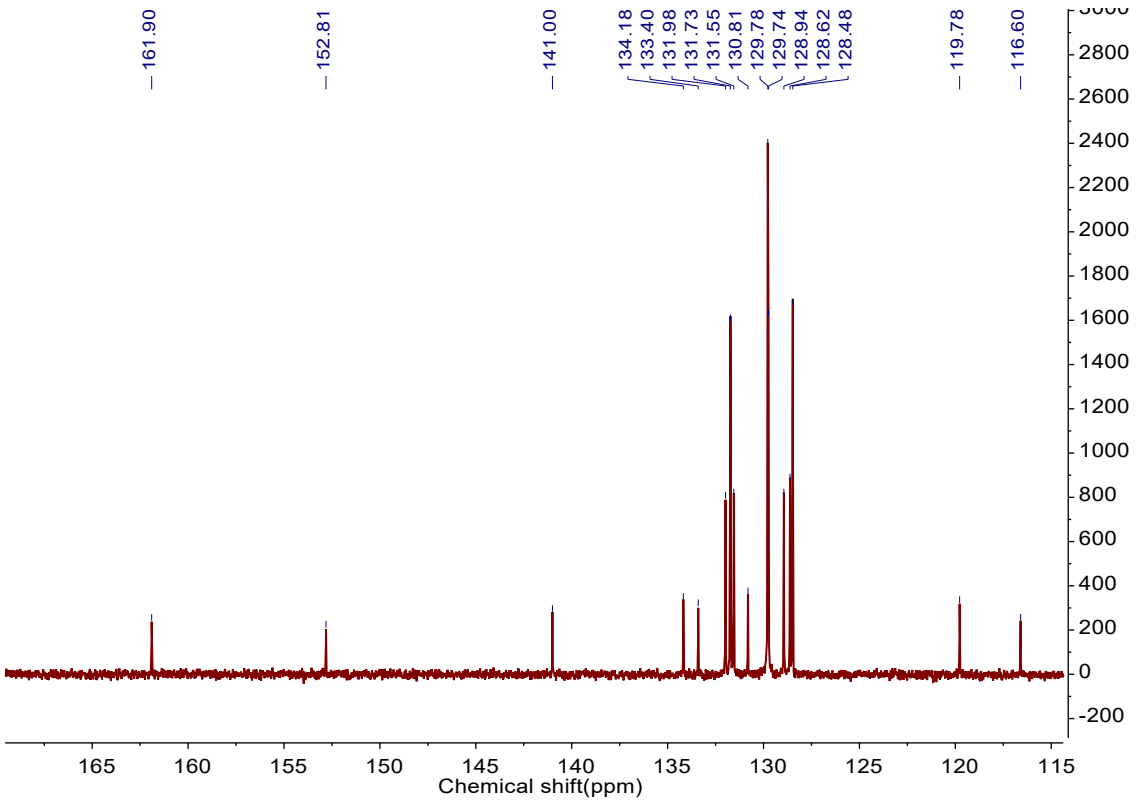

Figure S22. The ^{13}C NMR spectra of PADA-Br in CD_2Cl_2.

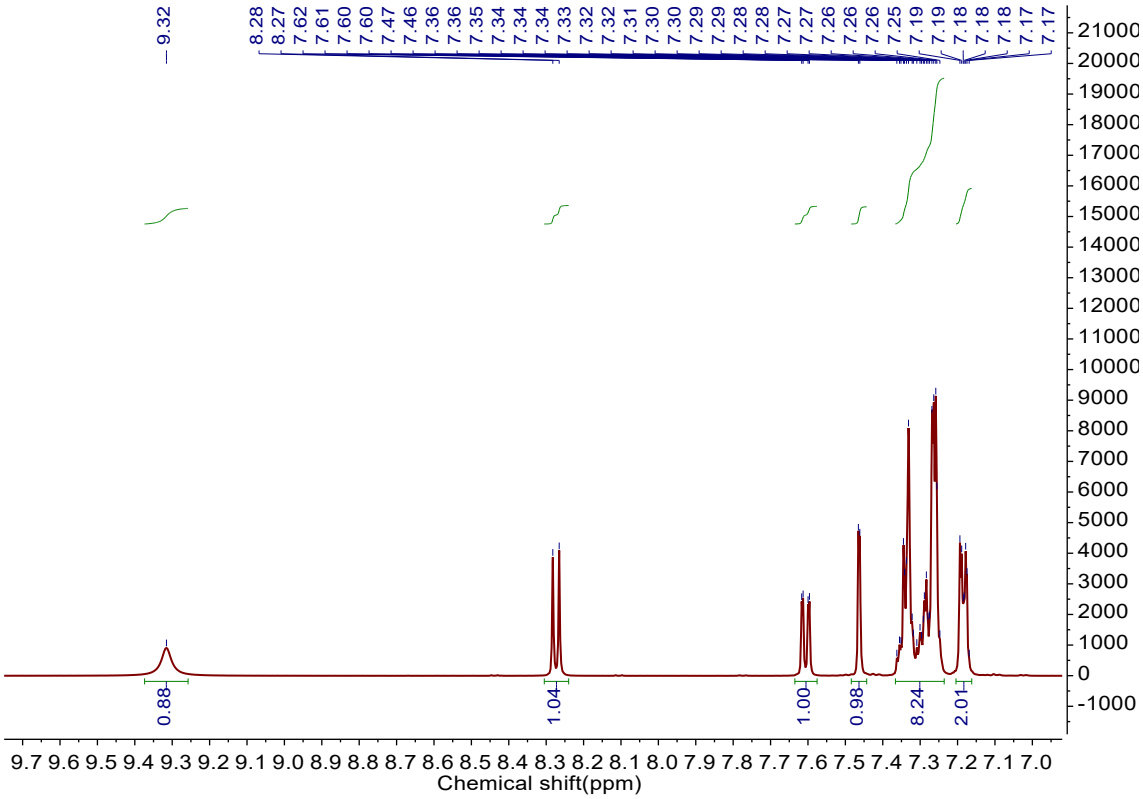

Figure S23. The ^{1}H NMR spectra of PADH-Br in CD_2Cl_2.

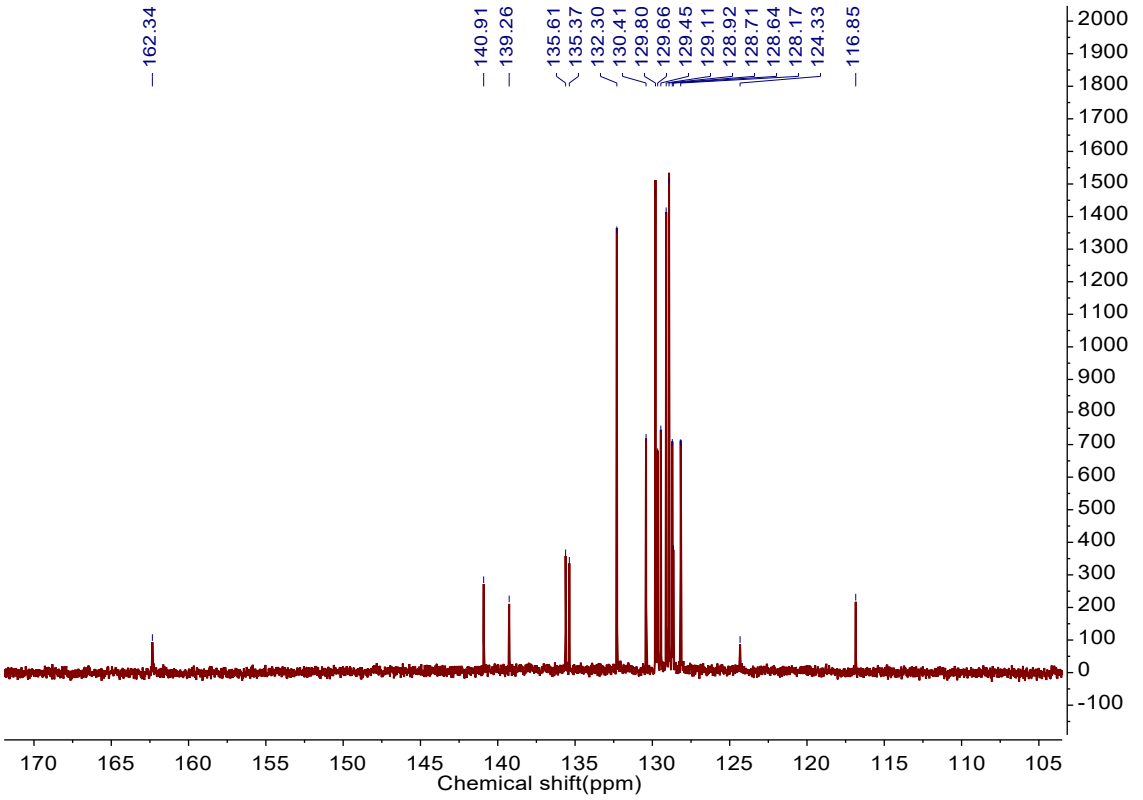

Figure S24. The ^{13}C NMR spectra of PADH-Br in CD_2Cl_2.

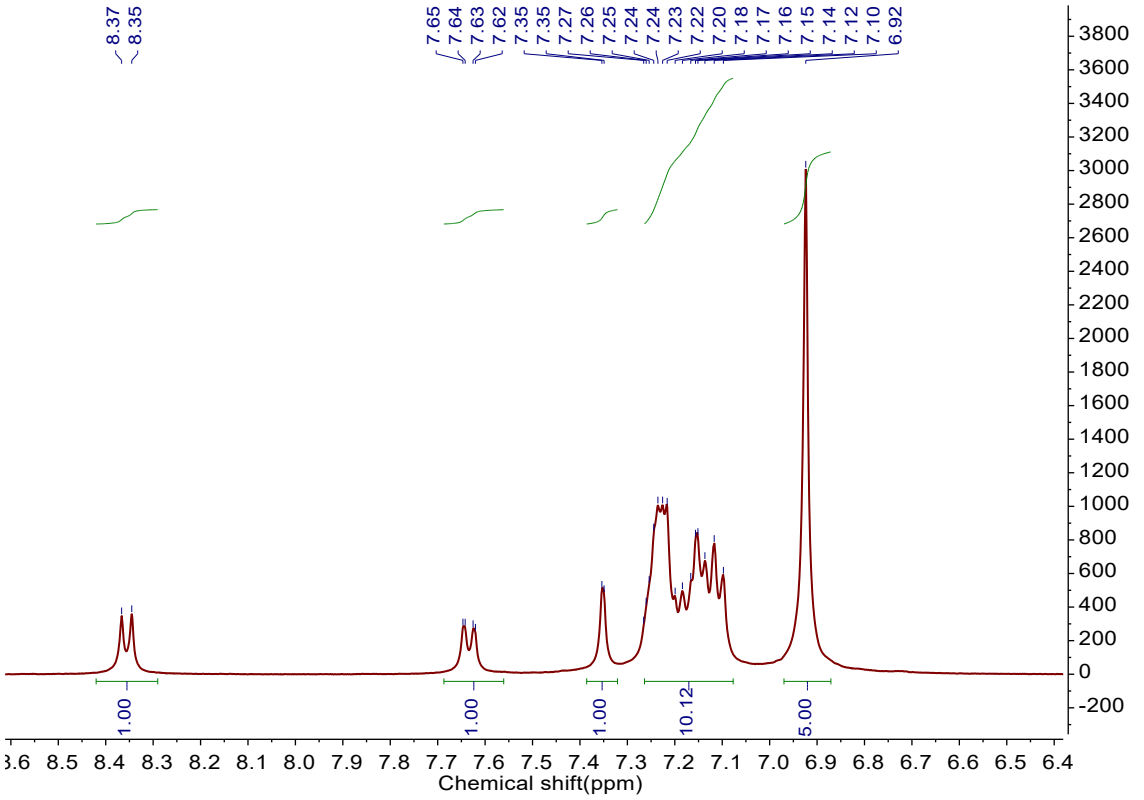

Figure S25. The ^{1}H NMR spectra of PADP-Br in CD_2Cl_2.

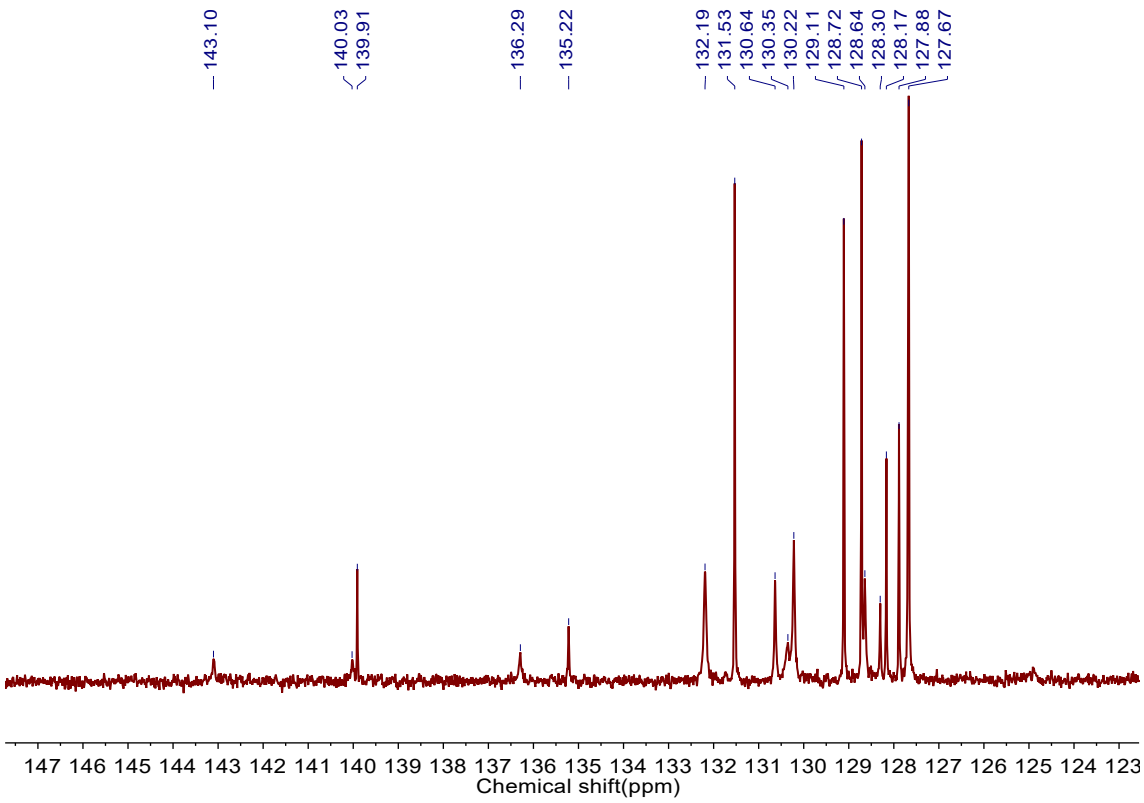

Figure S26. The ^{13}C NMR spectra of PADP-Br in CD_2Cl_2.

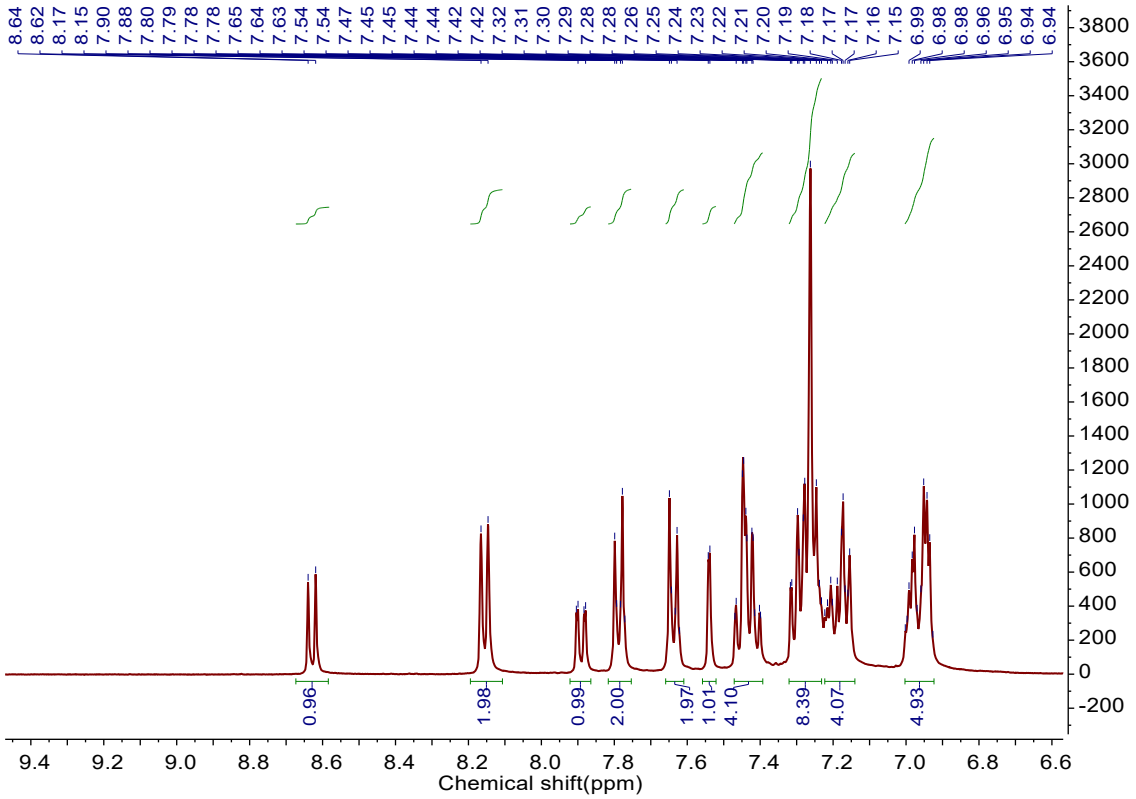

Figure S27. The ^{1}H NMR spectra of PADP-pCz in CD_2Cl_2.

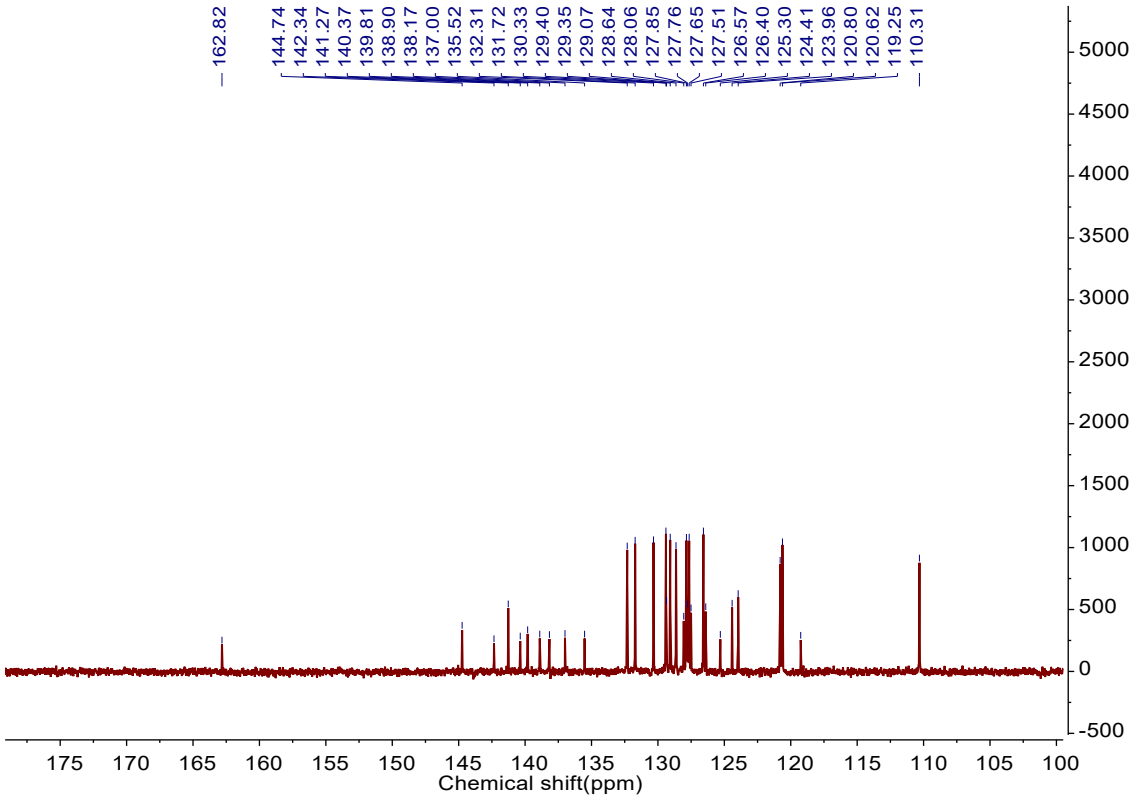

Figure S28. The ^{13}C NMR spectra of PADP-pCz in CD_2Cl_2.

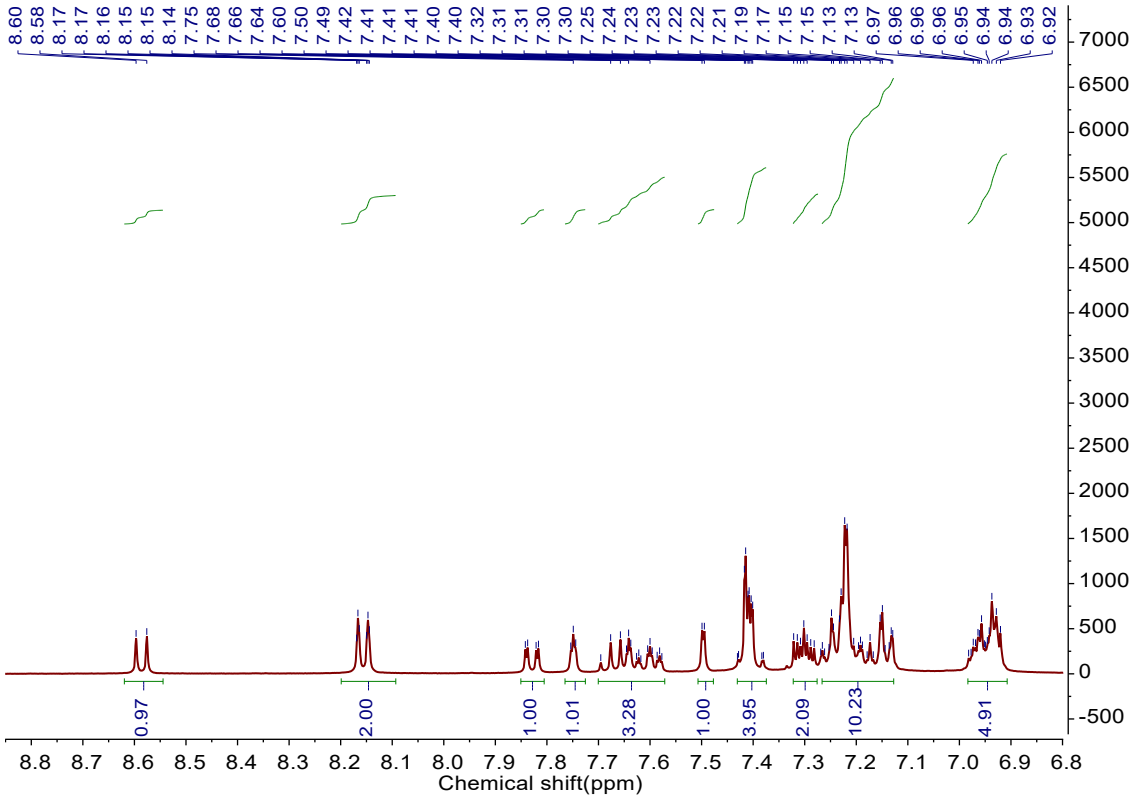

Figure S29. The ^{1}H NMR spectra of PADP-mCz in CD_2Cl_2.

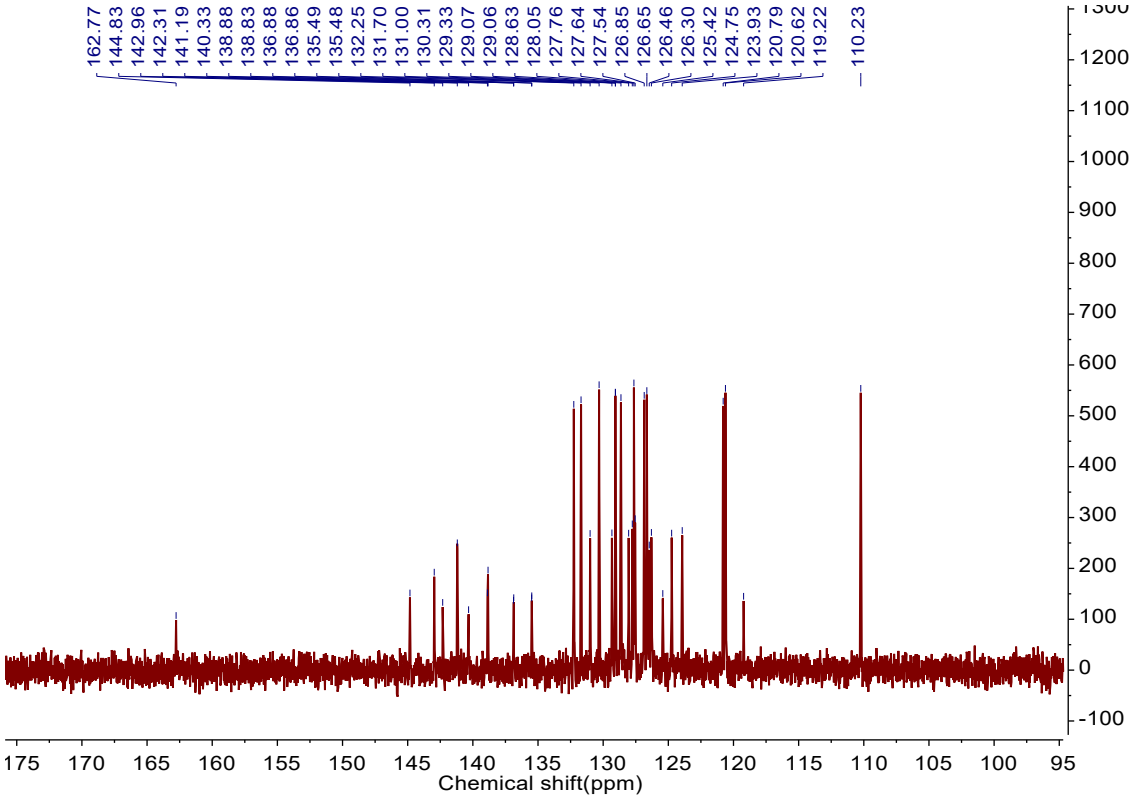

Figure S30. The ^{13}C NMR spectra of PADP-mCz in CD_2Cl_2.

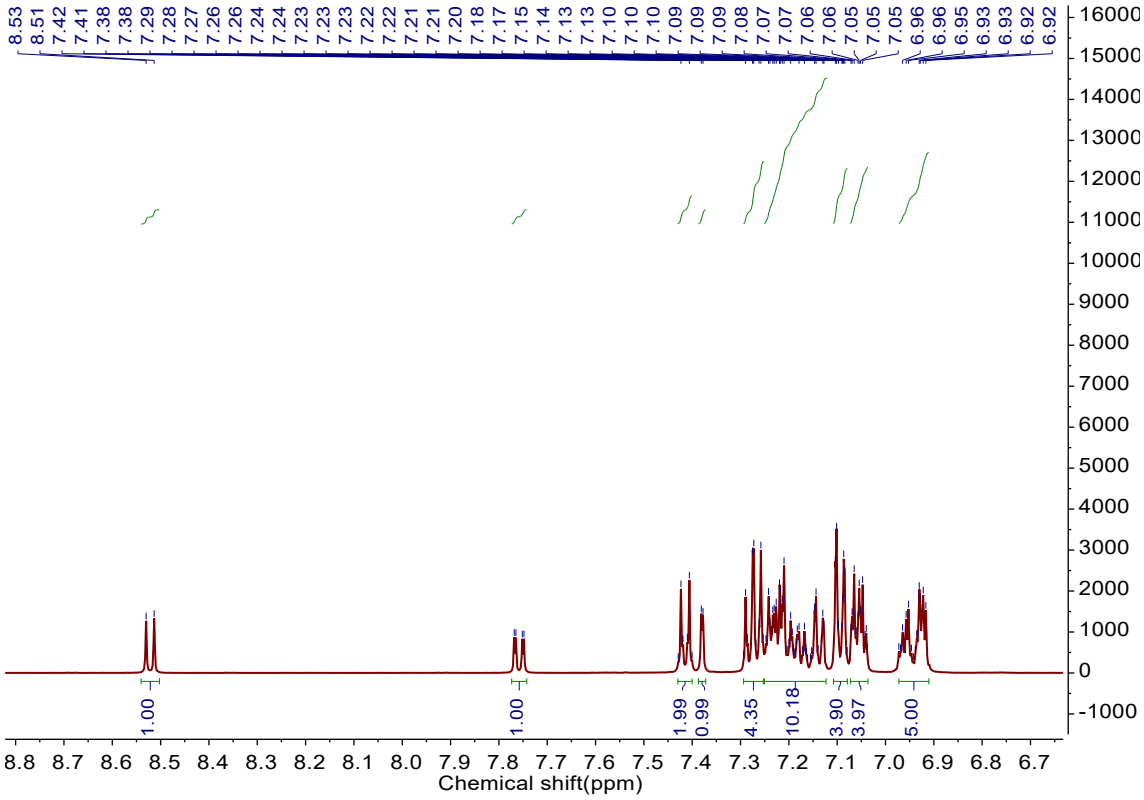

Figure S31. The ^{1}H NMR spectra of PADP-TPA in CD_2Cl_2.

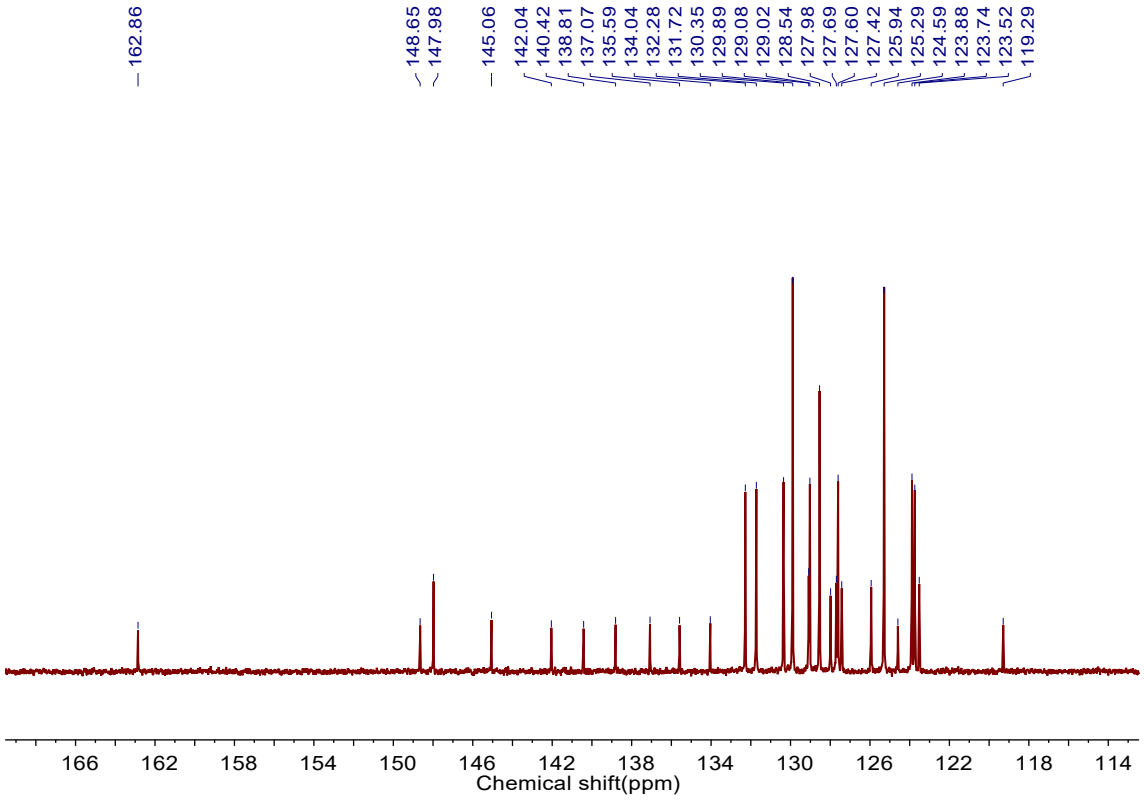

Figure S32. The ^{13}C NMR spectra of PADP-TPA in CD_2Cl_2.

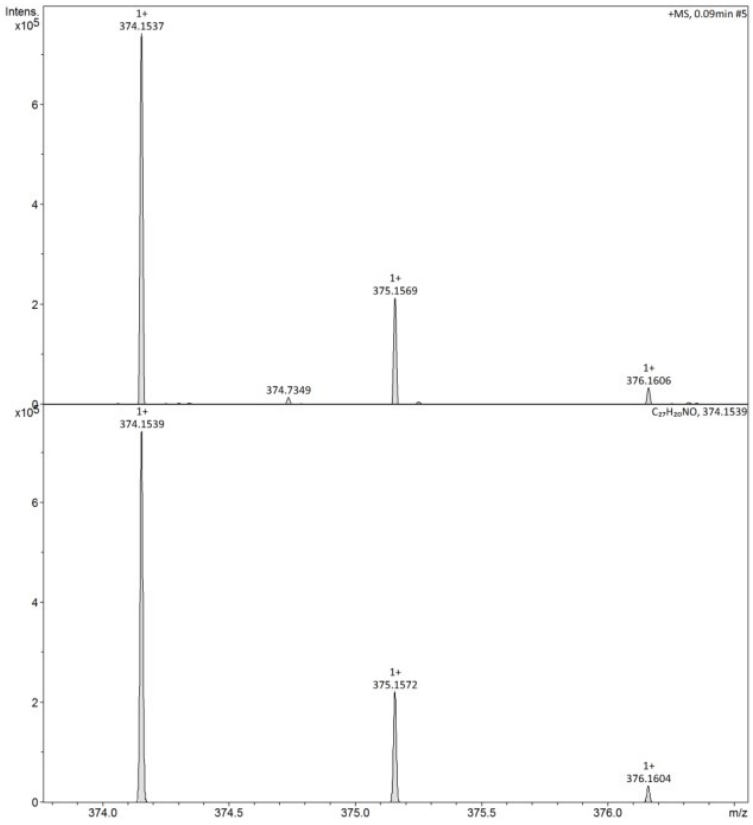

Figure S33. High resolution mass spectra (HRMS) of PADP.

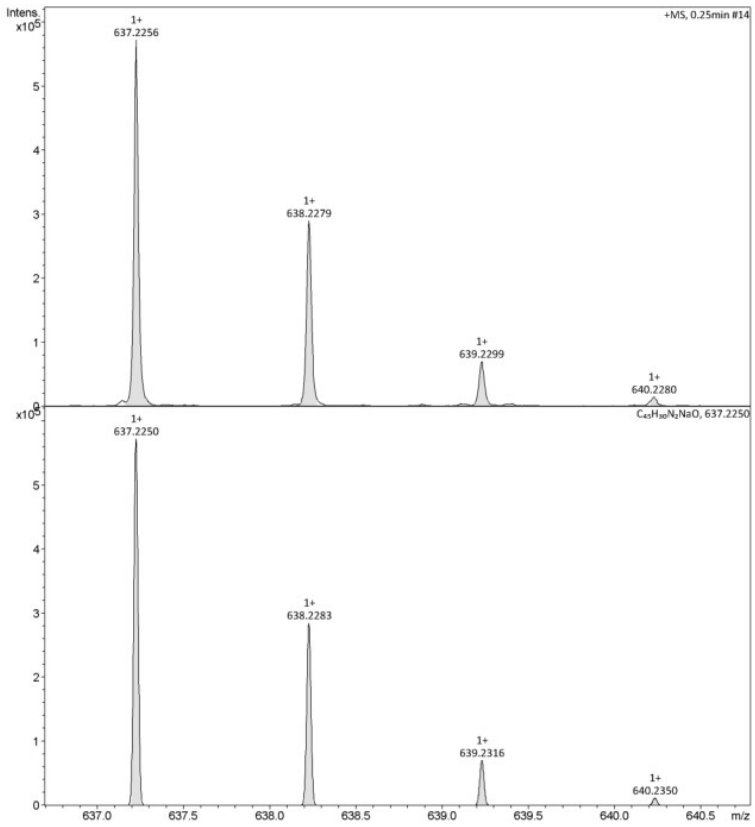

Figure S34. High resolution mass spectra (HRMS) of PADP-pCz.

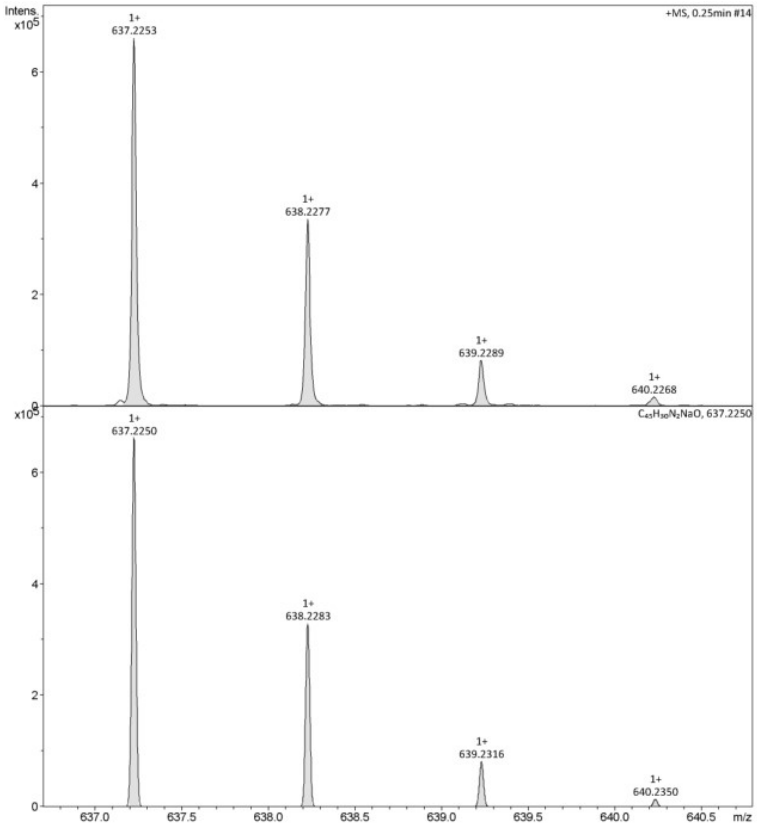

Figure S35. High resolution mass spectra (HRMS) of PADP-mCz.

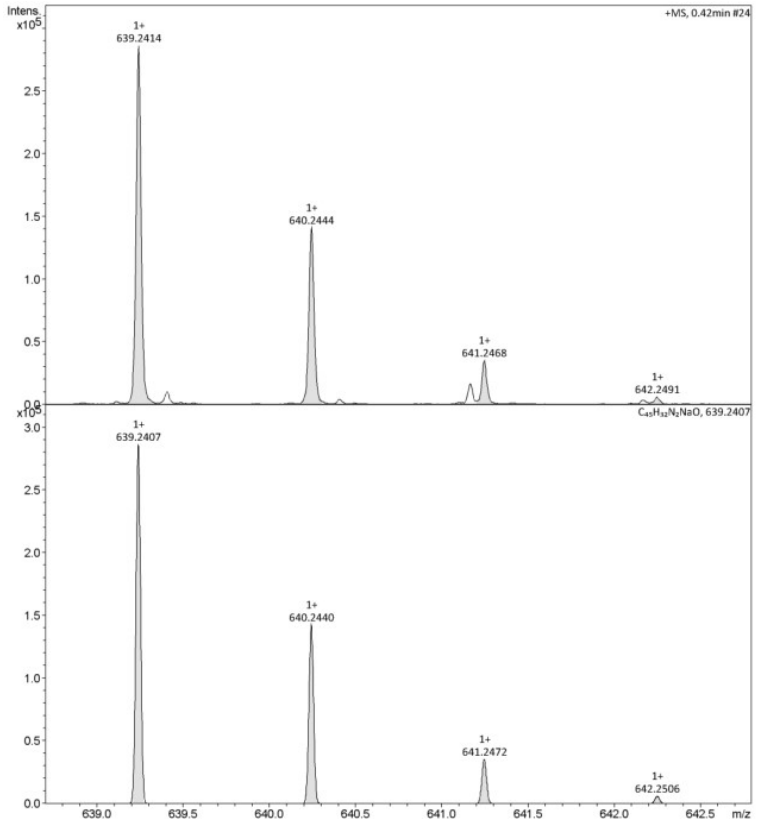

Figure S36. High resolution mass spectra (HRMS) of PADP-TPA.

S-8 Reference

[1] A. Islam, D. Zhang, L. Hong, H. Cui, Q. Wei, L. Duan, R. Peng, X. Ouyang, Z. Ge, *J. Photochem. Photobiol. A: Chemistry* 2018, **359**, 87.

[2] J. Huang, N. Sun, Y. Dong, R. Tang, P. Lu, P. Cai, Q. Li, D. Ma, J. Qin, Z. Li, *Adv. Funct. Mater*. 2013, **23**, 2329.

[3] J. Yang, J. Huang, N. Sun, Q. Peng, Q. Li, D. Ma, Z. Li, *Chemistry* 2015, **21**, 6862.

[4] C. Wang, L. Li, X. Zhan, Z. Ruan, Y. Xie, Q. Hu, S. Ye, Q. Li, Z. Li, *Sci. Bull*. 2016, **61**, 1746.

[5] W. Feng, Q.Su, Y. Ma, Zoran Džolić, F. Huang, Z. Wang, S. Chen, B. Z. Tang, *J. Org. Chem*. 2020, **85**, 158−167.

[6] L. Pan, H. Wu, J. Liu, K. Xue, W. Luo, P. Chen, Z. Wang, A. Qin, B. Z. Tang, *Adv. Optical Mater*. 2019, **7**, 1801673.

[7] H. Wu, J. Zeng, Z. Xu, B. Zhang, H. Zhang, Y. Pan, Z. Wang, D. Ma, A. Qin B. Z. Tang, *J. Mater. Chem. C* 2019, **7**, 13047—13051.

[8] H. Wu, G. Li, J. Luo, T. Chen, Y. Ma, Z. Wang, A. Qin, B. Z. Tang, *Adv.Optical Mater.* 2021, **9**, 2101085.

[9] Z.Xu, J. Gu, X. Qiao, A. Qin, B. Z. Tang, D. Ma, *ACS Photonics* 2019, **6**, 767−778.

[10] P. Han, C. Lin, D.Ma, A. Qin, B. Z. Tang, *ACS Appl. Mater. Interfaces* 2020, **12**, 46366−4637.

[11] C. Lin, P. Han, S. Xiao, F. Qu, J. Yao, X. Qiao, D. Yang, Y. Dai, Q. Sun, D. Hu, A. Qin, Y. Ma, B. Z. Tang, D. Ma, *Adv. Funct. Mater.* 2021, **31**, 2106912.

[12] P. Han, Z. Xu, C. Lin, D. Ma, A. Qin, B. Z. Tang, *J. Mater. Chem. C* 2020, **8**, 7012—7018.

[13] M. Bian, Z. Zhao, Y. Li, Q. Li, Z. Chen, D. Zhang, S. Wang, Z. Bian, Z. Liu, L. Duan, L. Xiao, *J. Mater. Chem. C* 2018, **6**, 745—753.

[14] Y. Cai, C. Shi, H. Zhang, B. Chen, K. Samedov, M. Chen, Z. Wang, Z. Zhao, X. Gu, D. Ma, A. Qin, B. Z. Tang, *J. Mater. Chem. C* 2018, **6**, 6534—6542.

[15] J. Yang, Q. Guo, Z. Ren, X. Gao, Q. Peng, Q. Li, D. Ma, Z. Li, *J. Mater. Chem. C* 2017, **5**, 6185—6192.

[16] J. Huang, N. Sun, J.Wang, R. Tang, X. Li, J. Dong, Q. Li, D. Ma, Z. Li, Isr. J. *Chem.* 2014,

54, 931–934.

[17] S. Liu, F. He, H. Wang, H. Xu, C, Wang, F. Li, Y. Ma, *J. Mater. Chem.* 2008, **18**, 4802–4807.

[18] W. Qin, Z. Yang, Y. Jiang, J. W. Y. Lam, G. Liang, H. S. Kwok, B. Z. Tang, *Chem. Mater*. 2015, **27**, 3892−3901.

[19] J. Yang, N. Sun, J. Huang, Q. Li, Q. Peng, X. Tang, Y. Dong, D. Ma, Z. Li, *J. Mater. Chem*. *C* 2015, **3**, 2624–2631.

[20] X. Zhan, N. Sun,Z. Wu, J. Tu, L. Yuan, X. Tang, Y. Xie, Q. Peng, Y. Dong, Qi. Li, D. Ma, Z. Li, *Chem. Mater.* 2015, **27**, 1847−1854.

[21] X. Zhan, Z. Wu, Y. Lin, Y. Xie, Q. Peng, Q. Li, D. Ma, Z. Li, *Chem. Sci*. 2016, **7**, 4355–4363.

[22] J. Lou, G. Li, X. Guo, B. Li, D. Yang, H. Zhang, Z. Wang, B. Z. Tang, *Small* 2024, **20**, 2308468.